Gravity-driven flow over heated, porous, wavy surfaces

K. A. Ogden,[1,a)] S. J. D. D'Alessio,[1,b)] and J. P. Pascal[2,c)]
[1]*Department of Applied Mathematics, University of Waterloo, Waterloo, Ontario N2L 3G1, Canada*
[2]*Department of Mathematics, Ryerson University, Toronto, Ontario M5B 2K3, Canada*

(Received 5 May 2011; accepted 30 August 2011; published online 16 December 2011)

The method of weighted residuals for thin film flow down an inclined plane is extended to include the effects of bottom waviness, heating, and permeability in this study. A bottom slip condition is used to account for permeability and a constant temperature bottom boundary condition is applied. A weighted residual model (WRM) is derived and used to predict the combined effects of bottom waviness, heating, and permeability on the stability of the flow. In the absence of bottom topography, the results are compared to theoretical predictions from the corresponding Benney equation and also to existing Orr-Sommerfeld predictions. The excellent agreement found indicates that the model does faithfully predict the theoretical critical Reynolds number, which accounts for heating and permeability, and these effects are found to destabilize the flow. Floquet theory is used to investigate how bottom waviness influences the stability of the flow. Finally, numerical simulations of the model equations are also conducted and compared with numerical solutions of the full Navier-Stokes equations for the case with bottom permeability. These results are also found to agree well, which suggests that the WRM remains valid even when permeability is included. [doi:10.1063/1.3667267]

I. INTRODUCTION

Gravity-driven flow down an inclined plane has been studied extensively on various levels: experimentally, theoretically, and numerically.[1–42] Film flow down an inclined plane with bottom heating has also been reported in several investigations.[43–53] In addition, the stability associated with flow down a porous inclined plane with and without heating was studied in Refs. 54–60.

Several recent studies have investigated the interaction of thermocapillary and inertial instabilities on thin fluid film flow down a heated impermeable incline. The common approach is to assume a linear variation in surface tension with temperature, while the other fluid properties are taken to be constant. Kalliadasis *et al.*[46] made this assumption and used a first-order integral-boundary-layer model to study flow over an even incline having a constant bottom temperature that exceeds that of the surrounding fluid. Following that work, Ruyer-Quil *et al.*[50] and Scheid *et al.*[52] applied a more accurate second-order weighted residual model (WRM) to the even bottom problem, improving the critical Reynolds number predictions for the flow. Later, Trevelyan *et al.*[53] considered both constant temperature and constant heat flux bottom boundary conditions using a weighted residual model, and concluded that in the long wave limit, heating has a destabilizing effect on the flow in both cases. Most recently, the problem with both bottom heating and topography, with a constant temperature bottom boundary condition, was analyzed by D'Alessio *et al.*[43] using a second-order weighted residual model.

In an innovative early study of flow along a porous boundary, Beavers and Joseph[61] proposed, and experimentally verified, effective conditions to be prescribed at the fluid-porous interface of Poiseuille flow and Darcyan filtration. Pascal[55] made use of these conditions to carry out a linear stability analysis of inclined flow. In that study, under the assumption of sufficiently low permeability, the filtration velocity was deemed relatively negligible, resulting in a one-sided model for the inclined flow, with the effect of substrate filtration being captured by a slip-velocity condition prescribed at the fluid-porous interface. The accuracy of the one-sided model was recently investigated by Liu and Liu[54] who compared the results with those from equations that coupled the flow with Darcyan filtration through the porous medium. They found that the one-sided approach is qualitatively correct, and in fact quite accurate in a wide range of cases involving low to moderate permeability, particularly if the porous substrate layer is not too thick. A similar confirmation was obtained by Thiele *et al.*[58] whose two-sided model implements the Darcy-Brinkman equation and also involves the thermal effects associated with a heated substrate. The one-sided method has been implemented in several investigations. For example, Pascal[56] incorporated a non-Newtonian rheology into the one-sided model and employed a depth-integrating strategy in order to facilitate linear and nonlinear stability analyses of the flow. Sadiq and Usha,[60] on the other hand, concentrated on the Newtonian case and established a Benney-type equation on which a weakly nonlinear stability analysis was performed. Thermal effects were included by Sadiq *et al.*,[59] while Pascal and D'Alessio[57] adjusted the fluid-porous interface conditions to non-planar geometry and implemented a one-sided model for isothermal flow which encompasses the effects of uneven bottom topography.

[a)]Electronic mail: kaogden@math.uwaterloo.ca.
[b)]Author to whom correspondence should be addressed. Electronic mail: sdalessio@uwaterloo.ca.
[c)]Electronic mail: jpascal@ryerson.ca.

Previous investigations concerning the effect of thermocapillarity on the stability of inclined flow have discovered a strong dependence of the critical Reynolds number on the Marangoni number, the parameter measuring the magnitude of the applied temperature difference and the influence of temperature on surface tension. The decrease in the critical Reynolds number is significant even if the value of the Marangoni number is small; therefore, thermocapillarity is a relevant factor in many situations involving the instability of inclined non-isothermal flow. The objective of the present work is to establish and implement a theoretical model which incorporates thermocapillary effects combined with both bottom topography and bottom permeability. This model would thus provide a more realistic description of a greater number of practical problems. In the manufacturing processes, one often finds objects with uneven surfaces which undergo coating applications with thin fluid films. Undulations may be associated with a required surface pattern for the object or can be an unintended consequence of a fabrication flaw. In other circumstances involving free-surface flows, it is important to design a special shape of the substrate that will result in the desired effect with regard to the occurrence of flow instability.[9] In a heat exchanger, for example, the formation of interfacial waves would be welcomed since this would increase the surface area of the liquid-gas interface which facilitates the transfer of heat. The additional inclusion of substrate permeability into the flow model would further broaden the range of possible applications. A permeable bottom condition can very effectively describe flow over rough surfaces[59] as well as cases where the substrate is an outright porous material, as is often the case in printing and painting processes and in the coating of textiles.[9] A thorough understanding of the effect of bottom undulations and permeability on flow instability would be instrumental in determining the optimal design of the substrate. Corrugated substrates can potentially be made more effective in their role as flow stabilizing or destabilizing agents if constructed from porous material or with a rough surface.

This investigation assumes that heating occurs as a result of a temperature difference between the bottom surface and the ambient air. A one-sided model is adopted whereby the effect of the porous medium is replaced by the Beavers and Joseph[61] slip condition. The derived model equations for film flow, expressed in terms of the flow rate, film thickness, and free-surface temperature, are then used to predict the critical Reynolds number for the onset of instability over an even bottom. In addition, the corresponding Benney equation[4,62–64] is also derived and used to determine the instability threshold. The results are compared with those obtained by Sadiq *et al.*,[59] who used a perturbation solution to the Orr-Sommerfeld equation to find the critical Reynolds number for flow over a heated, porous, even bottom. For the case of a sinusoidal bottom, Floquet theory is applied to analyze the influence of bottom topography on the stability of the flow.

An important advantage offered by the model equations over the complete set of equations and boundary conditions is that the model equations can be solved numerically much faster than the full equations. A fractional step method is implemented to numerically advance the model equations in time. Nonlinear numerical simulations are carried out to verify the predictions of the linear theory and also to compute the evolution of the interfacial waves for unstable flows. Lastly, numerical solutions of the full Navier-Stokes equations, obtained using the CFX software package, are conducted and contrasted with the model solutions.

The remainder of the article is organized as follows. The governing equations along with the non-dimensionalization procedure are described in Sec. II, while the mathematical formulation of the model is described in Sec. III. Steady-state solutions are discussed in Sec. IV and analyses of the stability of the flow are presented in Secs. V and VI. Numerical solutions for unstable cases are reported in Sec. VII, while the conclusions of the work are summarized in Sec. VIII. Finally, an Appendix has been included to investigate the consequences of including a temperature-dependent density and viscosity.

II. GOVERNING EQUATIONS AND BOUNDARY CONDITIONS

The flow configuration is shown in Fig. 1. The x-z coordinate system is defined so that the x-axis is directed down the incline with the z-axis pointing into the fluid layer. The surface is inclined at an angle β with the horizontal. The thickness of the fluid layer is given by $h(x, t)$ and the bottom topography is denoted by $\zeta(x)$.

The flow is assumed to be two dimensional and laminar, and the fluid is taken to be viscous, incompressible, and Newtonian. All the fluid properties are assumed to be constant with the exception of surface tension which varies linearly with temperature. In the Appendix we consider, in addition, temperature variations in density and viscosity for flow down an impermeable even incline and demonstrate that even if these variations are relatively significant, only the variation in surface tension affects the instability threshold.

The equations governing the problem are the continuity, momentum, and energy equations. Non-dimensional parameters appearing in the equations include

$$Re = \frac{Q}{\nu}, \quad We = \frac{\sigma H}{\rho Q^2}, \quad Bi = \frac{\alpha_g H}{\rho C_p \kappa_T},$$

$$Ma = \frac{\gamma \Delta T}{\rho U^2 H}, \quad Pr = \frac{\nu}{\kappa_T}, \quad Pe = PrRe,$$

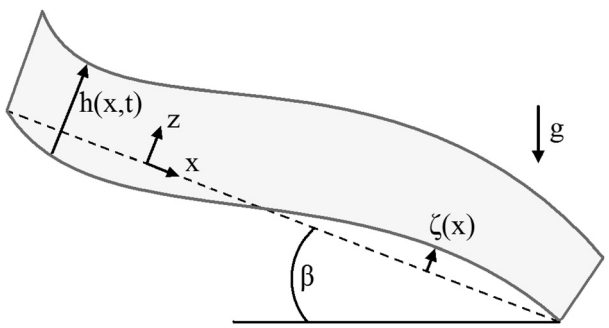

FIG. 1. Problem setup for the case with bottom topography.

and are known as the Reynolds, Weber, Biot, Marangoni, Prandtl, and Peclet numbers, respectively. Additional parameters are

$$\delta = \frac{H}{l},\ a_b,$$

which are the shallowness and the dimensionless bottom amplitude for the case of a wavy bottom. In dimensionless form, the bottom topography will vary according to

$$\zeta(x) = a_b \cos(2\pi x).$$

In this study, δ is assumed to be small, while a_b can be of order unity. It should be emphasized that a_b has been scaled with H, that is, $a_b = A_b/H$ where A_b is the dimensional bottom amplitude. Although $a_b = O(1)$, the bottom waviness is small relative to the wavelength of the bottom undulations, as $A_b = Ha_b = \delta a_b l$, so that the bottom amplitude is $O(\delta)$ compared to the wavelength. This means that the bottom undulations are slowly varying in the direction of flow. Here, Q is the characteristic volume flow rate, U is the characteristic velocity, H is the characteristic fluid layer thickness, and l is a characteristic length in the flow direction. For a wavy bottom, l will be taken to be the wavelength of the bottom topography. The fluid properties ν, ρ, α_g, c_p, κ_T, and σ denote the kinematic viscosity, density, interface heat transfer coefficient, specific heat, thermal diffusivity, and surface tension, respectively. Measuring the rate of decrease in surface tension with increasing temperature is the parameter γ. The change in temperature between the ambient surroundings (T_a) and the bottom surface (T_b) is given by $\Delta T = T_b - T_a$. For an impermeable, even bottom, the scales for the flow rate, Q, and the velocity, U, are related to the fluid thickness, H, through

$$Q = \frac{H^3 g \sin\beta}{3\nu}, \quad U = \frac{Q}{H} = \frac{H^2 g \sin\beta}{3\nu}.$$

This relation between Q and H is assumed in general, not just for the impermeable even bottom case. Lastly, the pressure scale is taken to be ρU^2.

With these non-dimensional parameters and scalings in place, the conservation equations can be simplified by assuming that $Re = O(1)$ and retaining terms up to second order in δ. It is well known that for isothermal flow along an even impermeable incline the instability threshold is given by $Re_{crit} = 5 \cot\beta/6$; thus, it is expected that the resulting governing equations will be suitable for investigating the stability of flows along sufficiently steep inclines. For sufficiently gentle inclinations, $\cot\beta$ becomes of order $1/\delta$ and large values of Re would have to be considered, which would render some of the discarded terms non-negligible. Further, for large Reynolds numbers, the flow becomes unstable with respect to shear waves of finite wavelength which is the dominant mode of instability if the inclination is small enough.[65] Under the assumption that the Reynolds numbers is $O(1)$ the non-dimensional governing equations, to $O(\delta^2)$, are[43]

$$\frac{\partial u}{\partial x} + \frac{\partial w}{\partial z} = 0, \tag{1}$$

$$\delta Re\left(\frac{\partial u}{\partial t} + u\frac{\partial u}{\partial x} + w\frac{\partial u}{\partial z}\right) = -\delta Re\frac{\partial p}{\partial x} + 3 + \frac{\partial^2 u}{\partial z^2} + \delta^2\frac{\partial^2 u}{\partial x^2}, \tag{2}$$

$$\delta^2 Re\left(\frac{\partial w}{\partial t} + u\frac{\partial w}{\partial x} + w\frac{\partial w}{\partial z}\right) = -Re\frac{\partial p}{\partial z} - 3\cot\beta + \delta\frac{\partial^2 w}{\partial z^2}, \tag{3}$$

$$\delta Pe\left(\frac{\partial T}{\partial t} + u\frac{\partial T}{\partial x} + w\frac{\partial T}{\partial z}\right) = \frac{\partial^2 T}{\partial z^2} + \delta^2\frac{\partial^2 T}{\partial x^2}, \tag{4}$$

which describe mass, x-momentum, z-momentum, and energy conservation, respectively. The non-dimensional dynamic conditions at the interface, $\eta = h + \zeta$, including terms to $O(\delta^2)$ are[43]

$$\left.\begin{aligned} p - \frac{2\delta}{Re}\frac{\partial w}{\partial z} + \delta^2(We - MaT)\frac{\partial^2(h+\zeta)}{\partial x^2} &= 0 \\ \frac{\partial u}{\partial z} - 4\delta^2\frac{\partial(h+\zeta)}{\partial x}\frac{\partial u}{\partial x} + MaRe\delta\left(\frac{\partial T}{\partial x} + \frac{\partial(h+\zeta)}{\partial x}\frac{\partial T}{\partial z}\right) &= 0 \end{aligned}\right\} \quad \text{at} \quad z = \eta. \tag{5}$$

The first expression ensures continuity of normal stress across the interface, while the second ensures a continuous tangential stress along the interface. The kinematic condition at the interface, $z = \eta$, is given non-dimensionally by

$$\frac{\partial h}{\partial t} = w - u\left(\zeta' + \frac{\partial h}{\partial x}\right). \tag{6}$$

Heat transfer at the interface occurs through convection and is described in dimensional form by

$$\vec{\nabla}T \cdot \hat{n} = -\frac{\alpha_g}{\rho c_p \kappa_T}(T - T_a) \quad \text{at} \quad z = \eta,$$

where $\hat{n}$ is the outward pointing normal to the surface. Temperature is non-dimensionalized using $\tilde{T} = (T - T_a)/(T_b - T_a)$. This boundary condition, when non-dimensionalized and suppressing the tildes, yields

$$-BiT\left(1 + \frac{\delta^2}{2}\left(\frac{\partial(h+\zeta)}{\partial x}\right)^2\right) = \frac{\partial T}{\partial z} - \delta^2\frac{\partial(h+\zeta)}{\partial x}\frac{\partial T}{\partial x} \quad \text{at} \quad z = \eta, \tag{7}$$

to $O(\delta^2)$.

The bottom boundary conditions include two expressions proposed by Beavers and Joseph.[61] For non-planar surfaces these have been extended by Saffman.[66] For example, the bottom slip condition as derived by Saffman in dimensional form is given by

$$\frac{\partial v^{||}}{\partial \hat{N}} = \vec{\nabla} v^{||} \cdot \hat{N} = \frac{\alpha}{\sqrt{\kappa}}(v^{||} - v_p^{||}),$$

where $v^{||}$ is the tangential component of the velocity along the bottom surface, $\hat{N}$ is the normal vector to the bottom surface, and the subscript p denotes a quantity in the porous medium. The permeability of the porous medium is denoted by κ, and α is a dimensionless parameter introduced by Beavers and Joseph.[61] In an attempt to simplify this condition, the ratio of the characteristic velocity scale in the porous medium, denoted by U_p, to that in the fluid layer is considered. Using $U_p = O(\kappa\rho \sin\beta/\nu)$ then yields

$$\frac{U_p}{U} = O\left(\left(\frac{\sqrt{\kappa}}{H}\right)^2\right) = O(\alpha^2\delta_1^2),$$

where

$$\delta_1 = \frac{\sqrt{\kappa}}{\sigma H},$$

and is also assumed to be small. The experiments of Beavers and Joseph[61] suggest that we can assume that $\alpha^2 = O(\delta)$. If it is further assumed that $\delta_1 = O(\delta)$, then it follows that $U_p/U = O(\delta^3)$. Since the model is second order in δ, this means that the velocities in the porous medium can be neglected. Thus, the above condition when non-dimensionalized simplifies to

$$\delta_1 \frac{\partial u}{\partial z} = u + \delta^2 \zeta' w \quad \text{at} \quad z = \zeta. \tag{8}$$

Condition (8) can be interpreted as a "slip-velocity" at the porous interface and is illustrated in Fig. 2. In reality there will be a boundary layer formed in the porous medium, which will guarantee that the velocity in the porous layer matches that in the fluid layer along the interface. The other bottom boundary condition comes from the continuity of normal velocity across the fluid – porous interface. This condition can be expressed as $v^{\perp} = v_p^{\perp}$ at $z = \zeta$ where $v^{\perp}$ denotes the velocity component normal to the bottom surface. When non-dimensionalized this boundary condition becomes

$$w = u\zeta' \quad \text{at} \quad z = \zeta, \tag{9}$$

to second order.

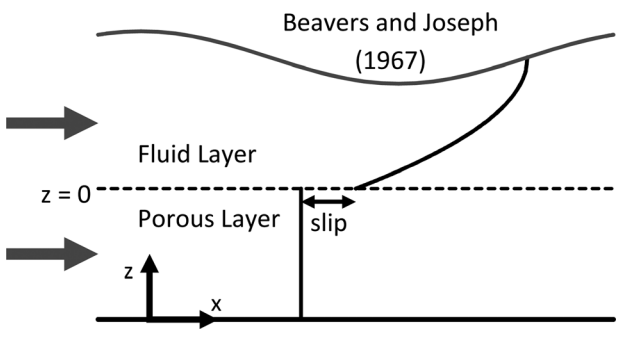

FIG. 2. Beavers and Joseph model for flow over a porous layer.[67]

A condition for the temperature at the bottom surface is also required. If the surface is maintained at a constant temperature of T_b, then it is clear from the proposed scaling that the condition becomes

$$T = 1 \quad \text{at} \quad z = \zeta. \tag{10}$$

Trevelyan *et al.*[53] consider both constant temperature and specified heat flux boundary conditions, and note that specifying the heat flux is more appropriate when modeling flows along a wall that loses heat to both the fluid and the ambient air. However, there are other applications where the constant temperature boundary condition may be more appropriate, such as in the problem considered by Nong *et al.*[68] involving a tear layer flowing over a contact lens. In this case, the eye would be maintained at a constant temperature as a result of the body heating the eye. This represents a prime example whereby a wavy, heated, porous bottom is combined with temperature dependent surface tension effects. Permeability is important because contact lenses are permeable. Heating affects the flow because the eye is heated by the body to a temperature greater than the surrounding air, and bottom topography comes into play through the curvature of the eye. Therefore, a model that combines all of these factors describes this flow more accurately than any of the previous models that only account for one or two of these factors. This is an important problem because instability and rupture of the tear layer over a contact lens is undesirable and uncomfortable for the contact lens wearer; therefore, the impact on stability presented by the degree of permeability, the temperature difference between the permeable layer and the surroundings, and the shape of the bottom topography are important in determining whether a particular design of contact lens will allow the tear layer to remain stable.

III. MODEL DEVELOPMENT

The method of weighted residuals, proposed by Ruyer-Quil and Manneville,[26] has been successfully applied to a host of problems involving heating and bottom topography. The goal here is to extend this method to include heating, permeability, and bottom topography.

First, the pressure is eliminated from Eqs. (2) and (3). This is easily accomplished by integrating the z-momentum equation from z to the free surface and applying the normal stress condition given by Eq. (5). The expression obtained for the pressure is then substituted into the x-momentum Equation (3). This leaves the continuity equation, a single momentum equation and the energy equation. Next, velocity and temperature profiles are assumed; as suggested by the steady-state solution, the velocity profile is chosen to have a parabolic shape given by

$$u(x,z,t) = \frac{3q}{2(h^3+3\delta_1 h^2)}b + \frac{\delta MaRe}{4h}\frac{\partial\theta}{\partial x}b_1 \quad \text{where}$$
$$b = (z-\zeta)(2h-z+\zeta) + 2\delta_1 h \quad \text{and} \tag{11}$$
$$b_1 = (z-\zeta)(2h-3(z-\zeta)).$$

It is worth noting that the parabolic profile stems from flow over an even bottom. The justification for applying it to a wavy bottom hinges on the fact that the bottom undulations are slowly varying in the direction of flow. Because of this, the deviation from the parabolic profile is expected to be small. In fact, D'Alessio *et al.*[43] have computed the steady-state profile to $O(\delta^2)$ and have found that the assumed parabolic profile matches the leading-order term exactly. The correction due to bottom waviness is $O(a_b\delta)$ and also takes on a similar parabolic profile. Thus, the deviation from the parabolic profile is indeed small, especially for small bottom amplitudes. The assumed parabolic profile satisfies the boundary conditions to $O(\delta)$ and the integral constraint,

$$\int_{\zeta}^{h+\zeta} u(x,z,t)dz = q(x,t), \tag{12}$$

where q is the dimensionless flow rate. Since it is not possible to simultaneously satisfy the bottom slip condition (8) to $O(\delta\delta_1)$ and condition (12), the slip condition is only satisfied to $O(\delta)$; this is acceptable because δ_1 is assumed to be $O(\delta)$, so the error is approximately $O(\delta^2)$. The temperature profile, on the other hand, is chosen to be linear to match its steady-state solution and is given by

$$T = 1 + \frac{\theta-1}{h}(z-\zeta), \tag{13}$$

where $\theta(x,t) = T(z=h+\zeta, x, t)$ is the interface temperature. As explained in connection with the assumed velocity profile, the deviation from the linear profile resulting from bottom waviness will be small. This profile satisfies the bottom temperature boundary condition, but not the interface condition (7). However, the interface condition is used in the development of the model when the equations are integrated in z, so its effect is included in the model. The momentum and energy equations are then multiplied by weight functions before integrating in z. In the spirit of the Galerkin method, the weight functions used are b from Eq. (11) for the momentum equation, and $(z-\zeta)$ for the energy equation. The last step involves integrating the equations across the fluid layer to eliminate the z-dependence. The final form of the model equations are

$$\frac{\partial h}{\partial t} + \frac{\partial q}{\partial x} = 0,$$
$$\begin{aligned}
\delta(h+2\delta_1)\frac{\partial q}{\partial t} &= \delta^3 hWe\left(\frac{5}{2}\delta_1 + \frac{5}{6}h\right)\left(\zeta''' + \frac{\partial^3 h}{\partial x^3}\right) + \frac{\delta^2}{Re}\left(\frac{9}{2}h\frac{\partial^2 q}{\partial x^2} - \frac{9}{2}\frac{\partial q}{\partial x}\frac{\partial h}{\partial x} - 6q\frac{\partial^2 h}{\partial x^2} - \frac{15}{4}q\zeta''\right.\\
&\left. + \frac{q}{h}\left(4\left(\frac{\partial h}{\partial x}\right)^2 - 5(\zeta')^2 - \frac{5}{2}\frac{\partial h}{\partial x}\zeta'\right)\right) + \delta^2 hReMa\left(\frac{1}{48}h^2\frac{\partial^2\theta}{\partial x\partial t} + \frac{15}{224}hq\frac{\partial^2\theta}{\partial x^2} + \frac{19}{336}h\frac{\partial q}{\partial x}\frac{\partial\theta}{\partial x} + \frac{5}{112}q\frac{\partial\theta}{\partial x}\frac{\partial h}{\partial x}\right)\\
&+ \delta\left(\frac{9}{7}\frac{q^2}{h}\frac{\partial h}{\partial x} - \frac{45}{16}\delta_1\frac{q^2}{h^2}\zeta' - \frac{5}{2}Ma\frac{\partial\theta}{\partial x}\left(\frac{h}{2}+\delta_1\right) - \frac{17}{7}q\frac{\partial q}{\partial x}\left(1+\frac{\delta_1}{h}\right)\right) + \delta\left(-\frac{5}{2}\frac{h\cot(\beta)}{Re}\left(\frac{\partial h}{\partial x}+\zeta'\right)(h+3\delta_1)\right)\\
&+ \frac{5}{2}\frac{h}{Re}(h+3\delta_1) - \frac{5}{2}\frac{q}{hRe},
\end{aligned} \tag{14}$$
$$\begin{aligned}
\delta h\frac{\partial\theta}{\partial t} &= \delta^2\left(-\frac{3}{2}\frac{Bi}{Pe}\theta\left(\zeta' + \frac{\partial h}{\partial x}\right)^2 + \frac{3}{40}MaReh^2\left(\frac{\partial\theta}{\partial x}\right)^2 + \frac{h}{Pe}\frac{\partial^2\theta}{\partial x^2} + \frac{1}{Pe}\frac{\partial\theta}{\partial x}\frac{\partial h}{\partial x}\right) + \delta^2(\theta-1)\\
&\times\left(\frac{3}{80}MaReh\left(h\frac{\partial^2\theta}{\partial x^2} + 2\frac{\partial\theta}{\partial x}\frac{\partial h}{\partial x}\right) + \frac{3}{Peh}\zeta'\frac{\partial h}{\partial x} + \frac{2}{Peh}\left(\frac{\partial h}{\partial x}\right)^2 - \frac{3}{2Pe}\zeta'' - \frac{1}{Pe}\frac{\partial^2 h}{\partial x^2}\right)\\
&+ \delta(\theta-1)\left(\frac{\delta_1}{h}\left(\frac{21}{40}\frac{\partial q}{\partial x} - \frac{21}{40}\frac{q}{h}\frac{\partial h}{\partial x} + \frac{9}{2}\frac{q}{h}\zeta'\right) - \frac{7}{40}\frac{\partial q}{\partial x}\right) + \delta\frac{q}{20}\frac{\partial\theta}{\partial x}\left(21\frac{\delta_1}{h} - 27\right) - \frac{3}{Peh}(\theta-1) - 3\frac{Bi}{Pe}\theta,
\end{aligned}$$

with the prime denoting differentiation with respect to x.

Although these equations appear to be more complicated than the original set of equations, they are easier to work with from analytical and numerical points of view since the boundary conditions are imbedded in these equations. Lastly, the even bottom case corresponds to $\zeta = 0$, the isothermal case can be recovered by setting $Bi = Ma = 0$, and the impermeable case can be generated by setting $\delta_1 = 0$.

IV. STEADY-STATE SOLUTIONS

The steady-state solutions for the even bottom case can be easily found from the model equations. From the continuity equation, q must be constant; in order to prescribe this value the scaling for q must be chosen. Two logical options exist. If $q = q_s = 1$ is chosen, then the momentum and energy equations give

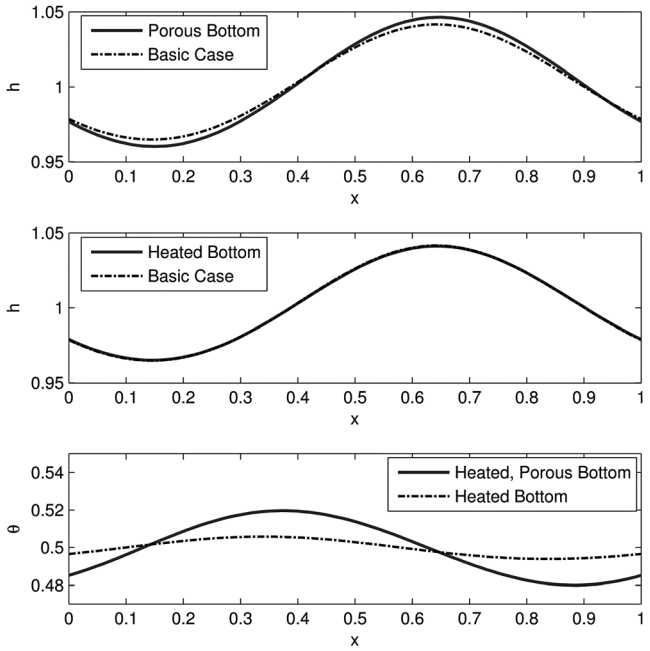

FIG. 3. Fluid thickness h and interface temperature θ over one bottom wavelength for $a_b = 0.1$, $\delta = 0.1$, cot $\beta = 1$, $We = 5$, and $Re = 1$; $\delta_1 = 0.1$ for cases with permeability parameter $\delta_1 = 0.1$ while for cases with heating $Ma = Bi = 1$.

$$h_s = 1 - \delta_1 + \delta_1^2 + O(\delta_1^3),$$
$$\theta_s = \frac{1}{1+Bi} + \frac{Bi}{(1+Bi)^2}\delta_1 - \frac{Bi}{(1+Bi)^3}\delta_1^2 + O(\delta_1^3). \tag{15}$$

Alternatively, q_s can be chosen so that $h_s = 1$; in this case, the steady-state solution for flow over an even bottom is

$$h_s = 1, \quad q_s = 1 + 3\delta_1, \quad \theta_s = \frac{1}{1+Bi}. \tag{16}$$

The expressions for h_s, q_s, and θ_s correspond to constant steady-state solutions for flow over an even incline. For variable bottom topography, the steady-state solution for q is still constant and equal to either $q_s = 1$ or $q_s = 1 + 3\delta_1$; however, the steady-state solutions for h and θ will vary with position.

The periodic steady-state solution for flow over a wavy bottom can be found using the Matlab routine bvp4c. Typical plots over one bottom wavelength showing the effect of heating and permeability on the fluid thickness and interface temperature are presented in Fig. 3 using the scaling $h_s = 1$. The basic case plotted in the top two panels represents the corresponding isothermal, impermeable case. The top panel shows the effect of adding a permeable bottom on the fluid layer thickness, which is to increase the overall variation. This is mainly driven by pressure and occurs because the fluid can penetrate the bottom boundary; fluid tends to flow into the boundary where the fluid layer is thinnest, and out of the bottom boundary where the fluid layer is thickest, thus exaggerating these extremes. This also explains why the temperature variation is greater for the porous bottom case, as seen in the bottom panel. Since bottom permeability increases the variation in fluid thickness, the interface temperature will also vary more across one bottom wavelength. Finally, the middle panel of Fig. 3 shows an impermeable case and reveals that heating has a negligible effect on the fluid thickness.

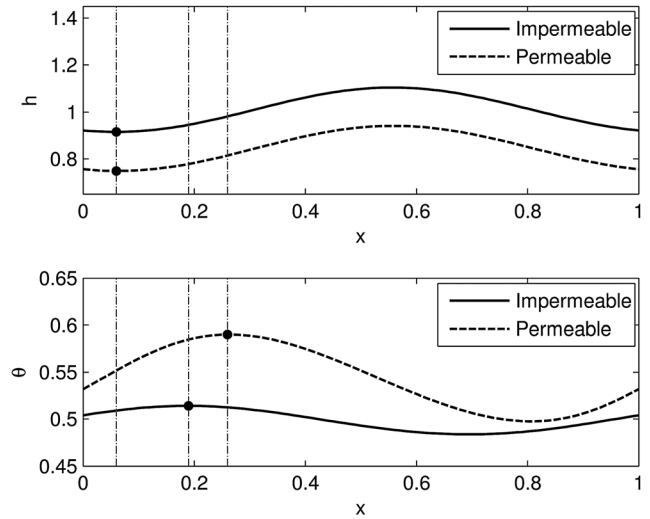

FIG. 4. Fluid thickness h and interface temperature θ over one bottom wavelength for $a_b = 0.1$, $\delta = 0.1$, cot $\beta = 1$, $We = 100$, $Bi = Ma = 1$, and $Re = 1$; for the cases with permeability parameter $\delta_1 = 0.1$.

Shown in Fig. 4 is the effect of permeability on the alignment of the peaks and troughs between h and θ for the scaling $q_s = 1$. For a stationary fluid, the interface temperature would be greatest where the fluid layer is thinnest because this is where the interface is closest to the heated bottom. Similarly, the interface temperature would be lowest where fluid layer is thickest. For a fluid in motion, though, these curves are shifted slightly so that the peak in interface temperature occurs slightly after the trough in fluid thickness, as illustrated in the plots. Adding permeability, however, shifts the θ curve even more, resulting in a greater gap between the point at which the fluid layer is thickest and the point at which the interface temperature is lowest. This finding makes sense since permeability has the effect of increasing the flow velocity. In this case, the gap increases by about 0.07 bottom wavelengths. This feature is also apparent in the unsteady numerical solutions to be presented in Sec. VII.

V. LINEAR STABILITY FOR AN EVEN BOTTOM

The critical Reynolds number for the even bottom problem with both bottom heating and permeability is determined using two different methods. One method involves deriving the Benney equation corresponding to this problem and then performing a linear stability analysis on this equation. Alternatively, a stability analysis of the WRM equations can also be carried out. The results from these two methods are compared to each other and also to the results obtained by Sadiq *et al.*[59] From these comparisons, the performance of the weighted residual model can be assessed. The expressions for the critical Reynolds number are also used to establish the impact of heating and bottom permeability on the stability of the flow.

A. Linear stability using the Benney equation

Deriving the Benney equation makes use of the governing equations (1)–(4) and accompanying boundary conditions (5)–(10) to generate an evolution equation for the fluid thickness, $h(x, t)$. In keeping with the expansion procedure introduced by Benney,[4] each of the primitive variables, u, w, p, and T, is expanded in powers of the shallowness parameter δ; for example, u is expanded in the series $u = u_0 + \delta u_1 + O(\delta^2)$. For the purposes of this analysis, only δ is treated as a small parameter. The smallness of δ_1 will not be exploited here; it was used mainly to simplify the bottom boundary conditions.

Substituting these expansions into the governing equations and boundary conditions leads to a hierarchy of problems at each order of δ. The first-order Benney equation requires only the $O(1)$ and $O(\delta)$ problems. Outlined below is the solution of the $O(1)$ problem. The governing equations at leading order are

$$\begin{aligned} \frac{\partial u_0}{\partial x} + \frac{\partial w_0}{\partial z} &= 0, \\ 3 + \frac{\partial^2 u_0}{\partial z^2} &= 0, \\ Re\frac{\partial p_0}{\partial z} + 3\cot\beta &= 0, \\ \frac{\partial^2 T_0}{\partial z^2} &= 0 \end{aligned} \tag{17}$$

The dynamic conditions at the free surface become

$$\left.\begin{aligned} p_0 &= 0 \\ \frac{\partial u_0}{\partial z} &= 0 \end{aligned}\right\} \quad \text{at} \quad z = h + \zeta, \tag{18}$$

and the free surface heat transfer condition gives

$$\frac{\partial T_0}{\partial z} = -BiT_0 \quad \text{at} \quad z = h + \zeta. \tag{19}$$

Lastly, the bottom boundary conditions are

$$\left.\begin{aligned} w_0 &= \zeta' u_0 \\ u_0 &= \delta_1 \frac{\partial u_0}{\partial z} \\ T_0 &= 1 \end{aligned}\right\} \quad \text{at} \quad z = \zeta. \tag{20}$$

Equations (17)–(20) can be easily solved for u_0, w_0, p_0, and T_0 and the solutions are

$$\begin{aligned} u_0 &= \frac{-3}{2}(z^2 + \zeta^2) + 3z(h + \zeta) - 3h\zeta + 3h\delta_1, \\ w_0 &= \frac{-3}{2}\left(\zeta' + \frac{\partial h}{\partial x}\right)(z - \zeta)^2 \\ &\quad + 3\left(\zeta' h - \delta_1 \frac{\partial h}{\partial x}\right)(z - \zeta) + 3\zeta' h\delta_1, \\ p_0 &= \frac{3\cot\beta}{Re}(z - \zeta - h), \\ T_0 &= 1 + (\zeta - z)\frac{Bi}{1 + hBi}. \end{aligned} \tag{21}$$

Continuing this procedure for the $O(\delta)$ problem yields expressions for u_1, w_1, p_1, and T_1. The first-order Benney equation is then obtained from the kinematic condition to which $O(\delta)$ is

$$\frac{\partial h}{\partial t} = w_0 - (u_0 + \delta u_1)\left[\frac{\partial h}{\partial x} + \zeta'\right] + \delta w_1. \tag{22}$$

The final Benney equation for the even bottom problem including both heating and bottom permeability is

$$\begin{aligned} &\frac{\partial h}{\partial t} + 6\delta_1 h\frac{\partial h}{\partial x} + \frac{\partial h^3}{\partial x} + \delta\frac{\partial}{\partial x}\left(\frac{6}{5}Re\left(h^6\frac{\partial h}{\partial x} + 6\delta_1 h^5\frac{\partial h}{\partial x}\right.\right. \\ &\left.\left. + \frac{25}{2}\delta_1^2 h^4\frac{\partial h}{\partial x}\right)\right) + \delta\frac{\partial}{\partial x}\left(\frac{MaReBi}{(1 + hBi)^2}h\frac{\partial h}{\partial x}\left(\frac{h}{2} + \delta_1\right)\right. \\ &\left. - \cot\beta(3\delta_1 h^2 + h^3)\frac{\partial h}{\partial x}\right) = 0. \end{aligned} \tag{23}$$

The fluid thickness h is next perturbed about the steady-state solution according to $h = h_s + \hat{h}$ where the perturbation, $\hat{h}$, is assumed to have the form, $\hat{h} = h_0 e^{ik(x-ct)}$. Substituting this into the Benney equation and linearizing in the perturbation produces a dispersion equation. The critical Reynolds number, Re_{crit}^{Ben}, is found from $\Im(c) = 0$ where $\Im(c)$ denotes the imaginary part of c. This leads to

$$\begin{aligned} Re_{crit}^{Ben} = &\frac{5}{6}\cot\beta \\ &\times\left[\frac{3\delta_1 h_s^2 + h_s^3}{h_s^6 + 6\delta_1 h_s^5 + \frac{25}{2}\delta_1^2 h_s^4 + \frac{5}{6}\frac{MaBi}{(1 + h_s Bi)^2}h_s\left(\frac{h_s}{2} + \delta_1\right)}\right]. \end{aligned} \tag{24}$$

For the scaling $q_s = 1$, the expression becomes

$$Re_{crit}^{Ben} = \frac{\frac{5}{6}\cot\beta}{1 + \frac{5MaBi}{12(1 + Bi(1 - \delta_1 + \delta_1^2))^2}(\delta_1^2 + 1) + \frac{7}{2}\delta_1^2}, \tag{25}$$

while for the scaling $h_s = 1$, the critical Reynolds number is given by

$$Re_{crit}^{Ben} = \frac{5}{6}\cot\beta\left[\frac{1 + 3\delta_1}{1 + 6\delta_1 + \frac{25}{2}\delta_1^2 + \frac{5MaBi}{12(1 + Bi)^2}(1 + 2\delta_1)}\right]. \tag{26}$$

This result has a similar form to the critical Reynolds number for flow over an isothermal impermeable surface given by $5\cot\beta/6$ (Refs. 3, 4, and 41), to the critical Reynolds number for flow over a heated impermeable surface given by[43]

$$\frac{\frac{5}{6}\cot\beta}{1 + \frac{5MaBi}{12(1 + Bi)^2}},$$

and also to that for isothermal flow over a permeable surface given by[55,57]

$$\frac{5}{6}\cot\beta\left[\frac{1+3\delta_1}{1+6\delta_1+\frac{25}{2}\delta_1^2}\right].$$

Expressions (25) and (26) account for the combined influence of heating and permeability, and it can be seen that heating and permeability acting either together or individually cause the critical Reynolds number to fall below the isothermal impermeable threshold of $5\cot\beta/6$, and hence destabilize the flow.

Lastly, presented in the Appendix is an extension of the problem considered in this section that includes a temperature-dependent density and viscosity, in addition to variable surface tension. The impact of these variable fluid properties on the stability of the flow is deduced using a similar analysis based on the corresponding Benney equation.

B. Linear stability using the model equations

An alternative method for determining the critical Reynolds number takes advantage of the WRM equations. Each flow variable in the model equations, h, q, and θ, is perturbed about its steady-state value as follows:

$$q = q_s + q_0 e^{ik(x-ct)}, \quad h = h_s + h_0 e^{ik(x-ct)},$$
$$\theta = \theta_s + \theta_0 e^{ik(x-ct)}.$$

These are then substituted into the model equations and linearized in the perturbations. The three equations are then combined to yield a dispersion equation. For neutral stability, the imaginary part of c is set to zero, whereas the real part is found to be $s = 3h_s(h_s + 2\delta_1)$. It is noted that the phase speed is close to 3, which is the value for isothermal, impermeable flow. The impact of permeability is seen to slightly increase the speed which is consistent with the general observation that permeability tends to increase the flow velocity. The critical Reynolds number is found to be

$$Re_{crit}^{WRM} = \frac{5}{6}\cot\beta\left[\frac{h_s^2(h_s+3\delta_1)}{h_s^3(h_s+2\delta_1)^3+\frac{1}{7}q_s^2-\frac{17}{7}h_s(h_s+2\delta_1)(h_s+\delta_1)q_s+\frac{5}{12}\frac{MaBi(h_s+2\delta_1)}{1+h_sB_i}h_s\theta_s}\right]. \tag{27}$$

For the scaling $q_s = 1$, the critical Reynolds number is

$$Re_{crit}^{WRM} = \frac{\frac{5}{6}\cot\beta}{1+\frac{5MaBi}{12(1+Bi)^2}\left(1+\frac{2Bi}{1+Bi}\delta_1+\frac{1+2Bi^2}{(1+Bi)^2}\delta_1^2\right)+\frac{29}{7}\delta_1^2}, \tag{28}$$

while for the scaling $h_s = 1$, the critical Reynolds number is

$$Re_{crit}^{WRM} = \frac{5}{6}\cot\beta\left[\frac{1+3\delta_1}{1+6\delta_1+\frac{92}{7}\delta_1^2+\frac{5MaBi(1+2\delta_1)}{12(1+Bi)^2}}\right]. \tag{29}$$

The critical Reynolds numbers obtained using this method are again similar in form to the isothermal, impermeable result, with a correction term to account for heating and permeability. They are also very similar to the corresponding expressions obtained using the Benney equation.

TABLE I. Comparison of critical Reynolds numbers for limiting cases to Orr-Sommerfeld results.

Limiting case	Re_{crit}^{WRM}	Re_{crit}^{Ben}	Re_{crit}^{Theory}
Isothermal and impermeable $Bi = Ma = \delta_1 = 0$	$\frac{5}{6}\cot\beta$	$\frac{5}{6}\cot\beta$	$\frac{5}{6}\cot\beta$
Impermeable $\delta_1 = 0$	$\frac{\frac{5}{6}\cot\beta}{1+\frac{5MaBi}{12(1+Bi)^2}}$	$\frac{\frac{5}{6}\cot\beta}{1+\frac{5MaBi}{12(1+Bi)^2}}$	$\frac{\frac{5}{6}\cot\beta}{1+\frac{5MaBi}{12(1+Bi)^2}}$
Isothermal $Bi = Ma = 0$	$\frac{5}{6}\cot\beta\left[\frac{1+3\delta_1}{1+6\delta_1+\frac{92}{7}\delta_1^2}\right]$	$\frac{5}{6}\cot\beta\left[\frac{1+3\delta_1}{1+6\delta_1+\frac{25}{2}\delta_1^2}\right]$	$\frac{5}{6}\cot\beta\left[\frac{1+3\delta_1}{1+6\delta_1+\frac{25}{2}\delta_1^2}\right]$

C. Comparison of linear stability results

The expressions for the critical Reynolds number obtained from the two methods can be compared to theoretical values for various limiting cases. This is done in Table I. The theoretical values, Re_{crit}^{theor}, have been obtained from perturbation expansion solutions of the Orr-Sommerfeld equation from previously published studies.[3,41,53,55,57] The scaling $h_s = 1$ is used for the case with permeability because the theoretical results were found using this scaling. The table shows that in the isothermal, impermeable limit, both the Benney and the WRM expressions reproduce the theoretical result. They also both yield the theoretical result in the impermeable limit. In the isothermal limit, the Benney equation gives the same result as that found by Pascal[55] and by Sadiq *et al.*[59] using the Orr-Sommerfeld equation; this is expected, though, as both the Benney and Orr-Sommerfeld equations emanate from the same governing equations and boundary conditions, without making any profile assumptions as was done in deriving the WRM. The weighted residual result differs only to second order in the small parameter δ_1. Because the WRM is second order in δ, this level of agreement is expected.

Sadiq *et al.*[59] also consider the problem with both heating and permeability, and obtain the following expression for the critical Reynolds number:

$$Re_{crit}^{Sad} = \frac{5}{6}\cot\beta\left[\frac{1+3\delta_1}{1+6\delta_1+\frac{25}{2}\delta_1^2+\frac{15}{2}\delta_1^3+\frac{5MaBi(1+2\delta_1)}{12(1+Bi)^2}}\right]. \tag{30}$$

They derive this result from a perturbation solution to the Orr-Sommerfeld equation using the scaling $h_s = 1$. This expression comes in close agreement with those given by Eqs. (26) and (29).

D. Effect of heating and porosity on stability

The effects of heating and permeability on the critical Reynolds number are illustrated in Figures 5–7. The critical Reynolds numbers using the scaling $q_s = 1$ as obtained from expressions (25) and (28) are plotted. Fig. 5 shows how increasing the permeability of the bottom surface affects the critical Reynolds number. The curves correspond to a particular case with bottom heating, although the same trend would be observed for other values of the Biot and Marangoni numbers, as well as for the isothermal case. The plot reveals that increasing the permeability of the bottom destabilizes the flow and hence decreases the critical Reynolds number. Increasing the permeability allows for slip along the bottom and, therefore, increases the overall velocity and volume flow rate, and the flow is therefore destabilized.

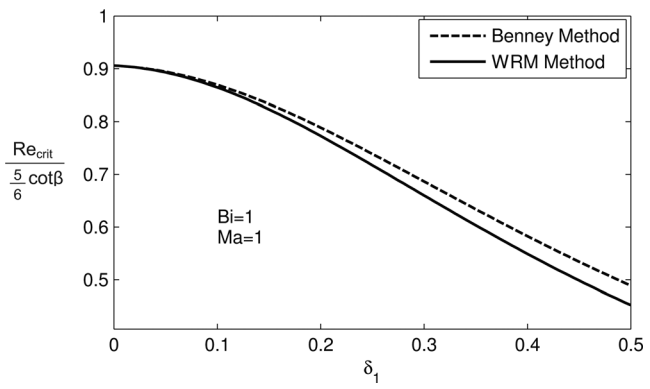

FIG. 5. Effect of increasing δ_1 on the critical Reynolds number.

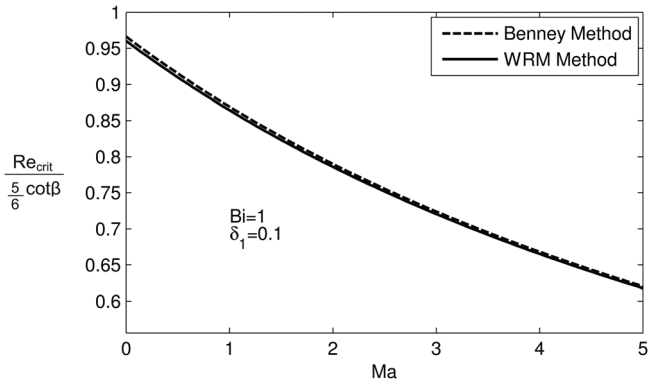

FIG. 6. Effect of increasing *Ma* on the critical Reynolds number.

It can be seen from Fig. 6 that increasing the Marangoni number also decreases the critical Reynolds number. The Marangoni number measures the variation in surface tension due to the temperature difference between the bottom surface and the surroundings. This result indicates that heating causes a variation in surface tension, which results in a less stable flow. The variation in surface tension causes fluid to be drawn to areas of higher surface tension. Since surface tension increases with decreasing temperature, the peaks of the disturbances will have higher surface tension since they are further from the bottom. Hence, fluid is drawn toward the peaks, causing the disturbances to grow and therefore destabilizing the flow.

Fig. 7 shows how varying the Biot number, while holding the Marangoni number and permeability parameter constant, affects the stability of the flow. In this case, there is a specific value of the Biot number, denoted by $Re_{crit,\min}^{WRM}$ and $Re_{crit,\min}^{Ben}$, at which the flow is most unstable; increasing the

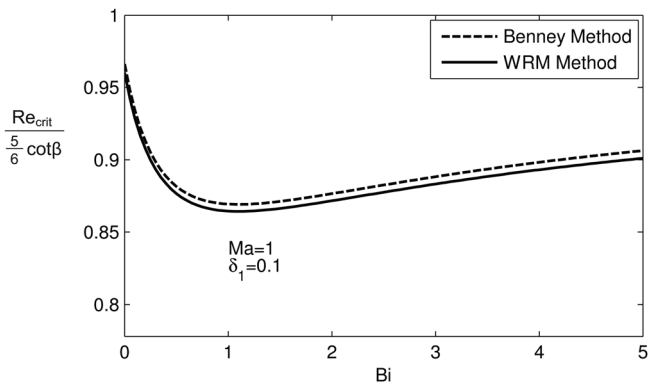

FIG. 7. Effect of increasing *Bi* on the critical Reynolds number.

Biot number from zero to that value destabilizes the flow, whereas increasing the Biot number beyond that value increases the critical Reynolds number bringing it closer to the isothermal limit.

The effect of heating and permeability on the stability of the flow can also be determined by differentiating the expression for the critical Reynolds number with respect to the parameters. For example, using the expression (25) gives

$$\frac{\partial Re_{crit}^{Ben}}{\partial Ma} = -\frac{5}{12}\frac{Bi(\delta_1^2+1)}{\left(1+\frac{5}{12}\frac{MaBi(\delta_1^2+1)}{(1+Bi(1-\delta_1+\delta_1^2)^2+\frac{7}{2}\delta_1^2}\right)^2(1+Bi(1-\delta_1+\delta_1^2))^2} < 0,$$

and so increasing the Marangoni number clearly decreases the critical Reynolds number. Similarly,

$$\frac{\partial Re_{crit}^{Ben}}{\partial \delta_1} = -\frac{\frac{5}{6}\frac{MaBi\delta_1}{(1+Bi(1-\delta_1+\delta_1^2))^2}-\frac{5}{6}\frac{MaBi^2(\delta_1^2+1)(2\delta_1-1)}{(1+Bi(1-\delta_1+\delta_1^2))^3}+7\delta_1}{\left(1+\frac{5}{12}\frac{MaBi(\delta_1^2+1)}{(1+Bi(1-\delta_1+\delta_1^2)^2+\frac{7}{2}\delta_1^2}\right)^2} < 0,$$

provided $\delta_1 < 0.5$; because δ_1 is assumed to be small and of order δ, this is expected to hold. Considering changes in the Biot number, however, it is easily shown that for the expression (25),

$$\frac{\partial Re_{crit}^{Ben}}{\partial Bi} = 0 \quad \text{when} \quad Bi = \frac{1}{1-\delta_1+\delta_1^2},$$

and attains a minimum value of

$$Re_{crit,min}^{Ben} = \frac{\frac{5}{6}\cot\beta}{1+\frac{7}{2}\delta_1^2+\frac{5Ma(1+\delta_1^2)}{48(1-\delta_1+\delta_1^2)}}.$$

This agrees with Fig. 7 which shows a minimum occurring near $Bi = 1$. A similar, but more complicated, result emerges for $Re_{crit,\min}^{WRM}$.

The critical Reynolds number is a minimum for a Biot number near unity because the interface temperature changes the most with changes in fluid thickness for that value. When the Biot number is much less than unity, the interface temperature is very close to the bottom surface temperature; therefore, changes in fluid thickness result in small interface temperature variations. On the other hand, when the Biot number is much larger than unity, the interface temperature is close to the ambient temperature, and again, changes in the fluid thickness cause only small changes in the interface temperature. Thus, in both of these cases, the variation in surface tension is small, and the destabilizing Marangoni effect is minimized. However, for a Biot number near unity, the temperature variation is largest and so surface tension varies the most along the interface; thus, the Marangoni effect is most pronounced. The Biot number at which this occurs varies slightly from unity in the presence of bottom permeability. However, this is simply due to the scaling. If the scaling $h_s = 1$ is used, then the value of the critical Biot number is exactly unity.

VI. LINEAR STABILITY WITH BOTTOM TOPOGRAPHY

To determine how bottom topography alters the instability threshold we analyze the system of Eq. (14) for the scaling $q_s = 1$ using

$$h = h_s(x) + \hat{h}, \quad q = 1 + \hat{q}, \quad \theta = \theta_s(x) + \hat{\theta},$$

where $h_s(x)$ and $\theta_s(x)$ denote the steady-state solutions. The linearized perturbation equations then take the form,

$$\frac{\partial \hat{h}}{\partial t} + \frac{\partial \hat{q}}{\partial x} = 0, \tag{31}$$

$$\frac{\partial \hat{q}}{\partial t} + f_1\frac{\partial^2 \hat{q}}{\partial x^2} + f_2\frac{\partial \hat{q}}{\partial x} + f_3\hat{q} + f_4\frac{\partial^3 \hat{h}}{\partial x^3} + f_5\frac{\partial^2 \hat{h}}{\partial x^2} + f_6\frac{\partial \hat{h}}{\partial x} + f_7\hat{h} + f_8\frac{\partial^2 \theta}{\partial xt} + f_9\frac{\partial^2 \hat{\theta}}{\partial x^2} + f_{10}\frac{\partial \hat{\theta}}{\partial x} = 0, \tag{32}$$

$$\frac{\partial \hat{\theta}}{\partial t} + g_1\frac{\partial^2 \hat{\theta}}{\partial x^2} + g_2\frac{\partial \hat{\theta}}{\partial x} + g_3\hat{\theta} + g_4\frac{\partial \hat{q}}{\partial x} + g_5\hat{q} + g_6\frac{\partial^2 \hat{h}}{\partial x^2} + g_7\frac{\partial \hat{h}}{\partial x} + g_8\hat{h} = 0, \tag{33}$$

where the coefficients $f_1(x)$–$f_{10}(x)$ and $g_1(x)$–$g_8(x)$ appearing in Eqs. (32) and (33) involve the steady-state solutions. For periodic bottom topography, these coefficients will also be periodic functions and this permits the use of Floquet theory to conduct the stability analysis. The perturbations are expanded in the truncated series given by

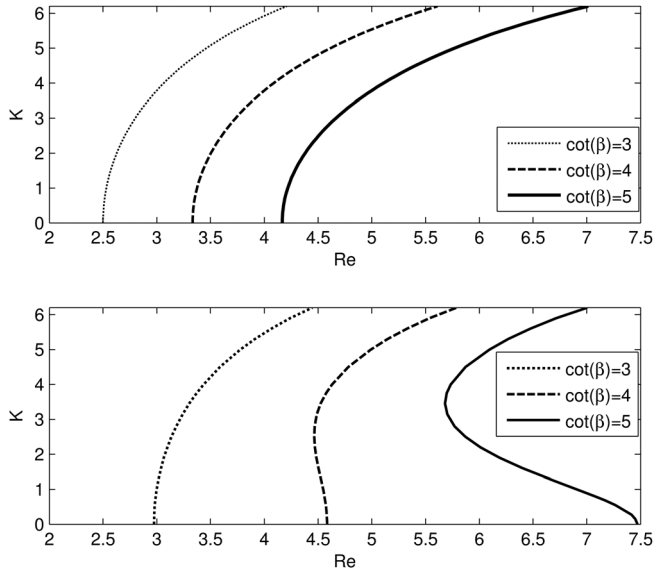

FIG. 8. Effect of increasing cot β for the isothermal, impermeable case where $\delta = 0.05$ and $We = 5$, with even bottom (top) and $a_b = 0.4$ (bottom).

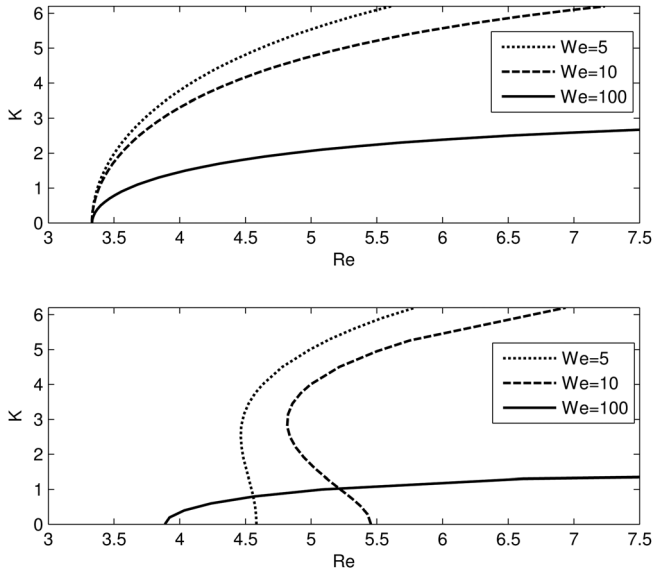

FIG. 10. Effect of increasing We for the isothermal, impermeable case where $\delta = 0.05$ and cot $\beta = 4$, with $a_b = 0$ (top) and $a_b = 0.4$ (bottom).

$$\hat{h} = e^{\omega t} e^{iKx} \sum_{n=-N}^{N} \hat{h}_n e^{i2\pi nx}, \quad \hat{q} = e^{\omega t} e^{iKx} \sum_{n=-N}^{N} \hat{q}_n e^{i2\pi nx},$$
$$\hat{\theta} = e^{\omega t} e^{iKx} \sum_{n=-N}^{N} \hat{\theta}_n e^{i2\pi nx}.$$

where K is the Bloch wavenumber of the perturbation. The coefficients $f_1(x)$–$f_{10}(x)$ and $g_1(x)$–$g_8(x)$ are expanded in a likewise truncated Fourier series. When these series are substituted into the linearized perturbation equations a system of equations results, which can be expressed as a generalized eigenvalue problem given by

$$\mathbf{A}\vec{V} = \omega \mathbf{B}\vec{V},$$

where $\mathbf{A}$ and $\mathbf{B}$ are $(6N+3) \times (6N+3)$ matrices and $\vec{V}$ is a vector of length $(6N+3)$ containing the coefficients $\hat{h}_n$, $\hat{q}_n$, $\hat{\theta}_n$ for $n = -N, \ldots, N$. The eigenvalues associated with this algebraic problem can be solved numerically using the MATLAB routine *eig*(**A**, **B**) to determine the temporal growth rate given by the real part of ω. This allows the critical Reynolds number for the onset of instability to be computed for specified values of the various parameters.

Figures 8–13 show the impact of varying the flow parameters on the neutral stability curve, plotted as K versus Re, with the scaling $q_s = 1$. In Fig. 8, neutral stability curves are shown for various angles of inclination for two bottom amplitudes. The curves show that decreasing the angle of inclination, which corresponds to increasing cot β, increases the critical Reynolds number, and shifts the entire curve to the right, toward higher Reynolds numbers. This is expected based on the expression for the critical Reynolds number for the basic case, $Re_{crit}^{even} = 5 \cot \beta / 6$. Furthermore, increasing

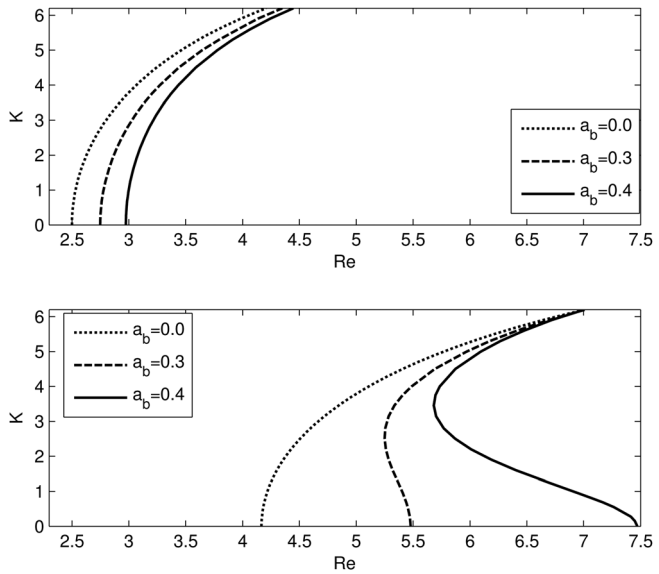

FIG. 9. Effect of increasing a_b for the isothermal, impermeable case where $\delta = 0.05$ and $We = 5$, with cot $\beta = 3$ (top) and cot $\beta = 5$ (bottom).

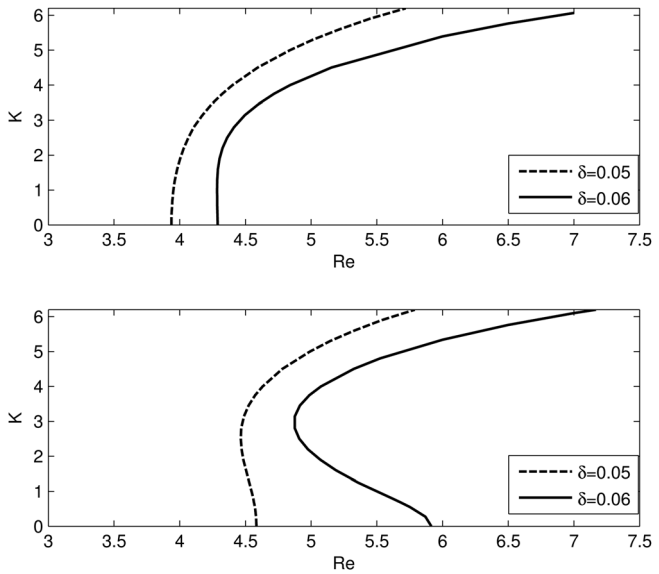

FIG. 11. Effect of increasing δ for the isothermal, impermeable case where $We = 5$ and cot $\beta = 4$, with $a_b = 0.3$ (top) and $a_b = 0.4$ (bottom).

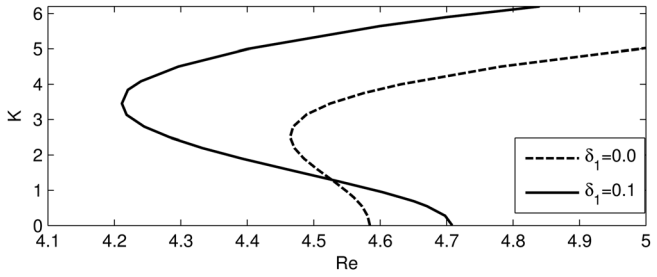

FIG. 12. Effect of increasing δ_1 for the case where $\delta = 0.05$, $We = 5$, $a_b = 0.4$, cot $\beta = 4$, and $Ma = Bi = 0$.

cot β, combined with a large bottom amplitude, changes the shape of the neutral stability curve, as seen in the bottom panel of Fig. 8. The critical Reynolds number is shifted away from the long-wave limit up to a non-zero wavenumber, resulting in shorter waves being the most unstable. This is most pronounced in the curve corresponding to cot $\beta = 5$ in the bottom panel of Fig. 8; here, the critical Reynolds number corresponds to a perturbation having a wavelength approximately equal to twice the bottom wavelength, which is unity for the scaling applied.

The effect of bottom topography is shown in Fig. 9, in which the curves from Fig. 8 have been rearranged to highlight the impact of varying the bottom topography. It can be seen that for each of the inclinations shown, increasing the bottom amplitude stabilizes the flow by shifting the curve to the right and therefore increasing the critical Reynolds number. The plots also show how increasing both the bottom amplitude and cot β changes the shape of the curve, as mentioned above.

The combined effect of surface tension and bottom topography on the stability of the flow is shown in Fig. 10. Shown in the top panel is a case with an even bottom; as expected surface tension does not affect the critical Reynolds number in the absence of bottom topography. However, the shape of the neutral stability curve is altered when surface tension is increased. The range of unstable wavelengths is reduced as surface tension is increased. The case with bottom topography shows that increasing the Weber number from $We = 5$ to $We = 10$ shifts the neutral stability curve to the right, which increases the critical Reynolds number and hence stabilizes the flow. This agrees with the predictions of the asymptotic analysis of D'Alessio *et al.*,[43] which indicated that when bottom topography and weak surface tension are combined, the flow rate is decreased, thereby stabilizing the flow. However, further increasing the Weber number actually reverses the combined effect of bottom topography and surface tension by destabilizing the flow. This result is also consistent with the reversal in stability reported in Ref. 43.

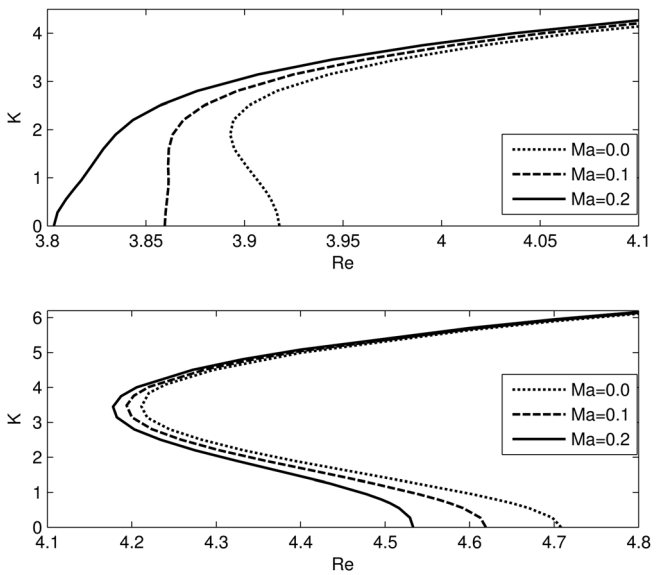

FIG. 13. Effect of increasing Ma for the case where $\delta = 0.05$, $We = 5$, cot $\beta = 4$, $Pr = 7$, $Bi = 1$, and $\delta_1 = 0.1$, with $a_b = 0.3$ (top) and $a_b = 0.4$ (bottom).

Shown in Fig. 11 is the effect of increasing the shallowness parameter δ, or increasing the fluid thickness relative to the wavelength of the bottom topography. Results are shown for two different values of bottom amplitude. For both amplitudes shown in the figure, increasing δ stabilizes the flow; that is, bottom topography having a shorter wavelength stabilizes the flow compared to that having a longer bottom wavelength. However, it must also be remembered that the underlying assumption that $\delta \ll 1$ puts a restriction on the bottom wavelength allowed since the bottom wavelength must be long compared to the fluid thickness. As already noted in Fig. 9, increasing the bottom amplitude stabilizes the flow for the small Weber number considered in this case.

The effect of bottom permeability on the stability of the flow is shown in Fig. 12. It can be seen that adding permeability decreases the critical Reynolds number, and thus, destabilizes the flow. Adding permeability also changes the shape of the neutral stability curve by increasing the wavenumber corresponding to the most unstable disturbance.

Finally, the Marangoni effect on the stability of the flow is shown in Fig. 13. Two sets of neutral stability curves are shown; in the top panel, the bottom topography is characterized by $a_b = 0.3$, and in the bottom panel, the bottom topography is described by $a_b = 0.4$. The curves show that increasing Ma while holding other parameters constant destabilizes the flow, even when bottom topography is included. Also, varying the Marangoni number can alter the value of the most unstable wavenumber, as seen in the top panel of Fig. 13. For flows with larger bottom amplitude, the shape of the curve can change such that the critical Reynolds number occurs for a non-zero wavenumber, as already witnessed in Fig. 8. For example, with $a_b = 0.3$ the critical Reynolds number can occur for a perturbation wavenumber of zero if the Marangoni number is sufficiently large, while this is not the case for $a_b = 0.4$. Comparing the top and bottom panels, it is clear that the Marangoni effect is more pronounced for small bottom amplitudes than it is for larger bottom amplitudes.

The neutral stability curves for flow over a wavy bottom show that most of the trends seen for an even bottom persist when bottom topography is added. One exception is that bottom waviness can change the wavenumber of the most unstable perturbation. Further, the plots confirm that adding bottom topography and weak surface tension stabilizes the

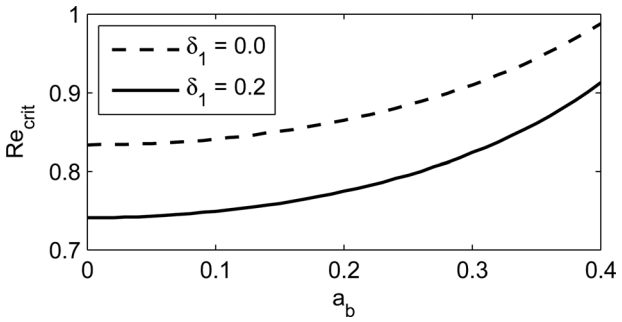

FIG. 14. Effect on the critical Reynolds number of increasing a_b for the case where $\delta = 0.05$, $We = 50$, $\cot\beta = 1$, and $Ma = Bi = 0$.

flow, while the combination of strong surface tension and bottom topography destabilizes the flow.

One last interesting feature worth presenting involves the interplay between permeability, surface tension, and bottom topography, and how this exchange affects the stability of the flow. This is captured in Figures 14 and 15, which plot the critical Reynolds number versus bottom amplitude for $We = 50$ and $We = 400$, respectively. Fig. 14 shows that for relatively small We, bottom permeability destabilizes the flow by shifting the entire curve downwards. As a_b increases though, the value of Re_{crit} also increases for both an impermeable and permeable bottom. Thus, once again bottom topography stabilizes the flow in the presence of moderately weak surface tension both with and without permeability. However, when We is increased considerably, Fig. 15 reveals that this is no longer the case. Here, for an impermeable bottom, increasing a_b destabilizes the flow, while for a permeable bottom it stabilizes the flow with Re_{crit} reaching a maximum value at $a_b \approx 0.3$. What is most interesting though, is that for $a_b \gtrsim 0.28$ the value of Re_{crit} for a permeable bottom exceeds that for the impermeable bottom. Thus, in the presence of sufficiently strong surface tension and for sufficiently large bottom amplitude, a permeable bottom can actually stabilize the flow. Adding heating to the cases shown in Figures 14 and 15 does not change these trends; heating simply shifts the curves downwards, and thus, destabilizes the flow as in the even bottom case.

VII. NUMERICAL SIMULATIONS

The weighted residual model equations, including heating, permeability and topography, are solved numerically

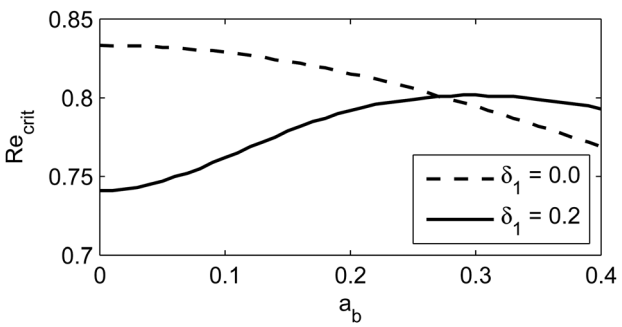

FIG. 15. Effect on the critical Reynolds number of increasing a_b for the case where $\delta = 0.05$, $We = 400$, $\cot\beta = 1$, and $Ma = Bi = 0$.

using the fractional step method,[69] as outlined in Ref. 43. In this method, the model equations are rewritten in the form which separates the advective and diffusive terms and solved in two steps. The WRM equations are expressed as

$$\frac{\partial h}{\partial t} + \frac{\partial q}{\partial x} = 0, \tag{34}$$

$$\frac{\partial q}{\partial t} + \frac{\partial}{\partial x}(\Psi_1) = \Psi_2, \tag{35}$$

and

$$\frac{\partial \phi}{\partial t} + \frac{\partial}{\partial x}(\Psi_3) = \Psi_4, \tag{36}$$

where the flow variable $\phi = h(\theta - 1)$ is used instead of θ. The functions Ψ_1, Ψ_3 represent advective terms while Ψ_2, Ψ_4 represent a combination of diffusive and source terms. These equations are solved in two steps. In the first step, the following system of equations involving only the advective terms is solved:

$$\frac{\partial h}{\partial t} + \frac{\partial q}{\partial x} = 0, \tag{37}$$

$$\frac{\partial q}{\partial t} + \frac{\partial}{\partial x}(\Psi_1) = 0, \tag{38}$$

$$\frac{\partial \phi}{\partial t} + \frac{\partial}{\partial x}(\Psi_3) = 0. \tag{39}$$

This system of hyperbolic conservation laws can be written compactly in vector form as

$$\frac{\partial \vec{U}}{\partial t} + \frac{\partial F(\vec{U})}{\partial x} = 0, \tag{40}$$

where

$$\vec{U} = \begin{bmatrix} h \\ q \\ \phi \end{bmatrix}, \quad F(\vec{U}) = \begin{bmatrix} q \\ \Psi_1 \\ \Psi_3 \end{bmatrix}. \tag{41}$$

The system is solved using MacCormack's explicit predictor-corrector scheme;[70] in the predictor step, a forward differencing scheme is used, while a backward differencing scheme is used in the corrector step. The method can be expressed as

$$\vec{U}_j^* = \vec{U}_j^n - \frac{\Delta t}{\Delta x}[F(\vec{U}_{j+1}^n) - F(\vec{U}_j^n)], \tag{42}$$

followed by

$$\vec{U}_j^{n+1} = \frac{1}{2}(\vec{U}_j^n + \vec{U}_j^*) - \frac{\Delta t}{2\Delta x}[F(\vec{U}_j^*) - F(\vec{U}_{j-1}^*)], \tag{43}$$

where $\vec{U}_j^n$ is the value of $\vec{U}$ at grid point j at time step n; Δt is the time step and Δx is the uniform grid spacing.

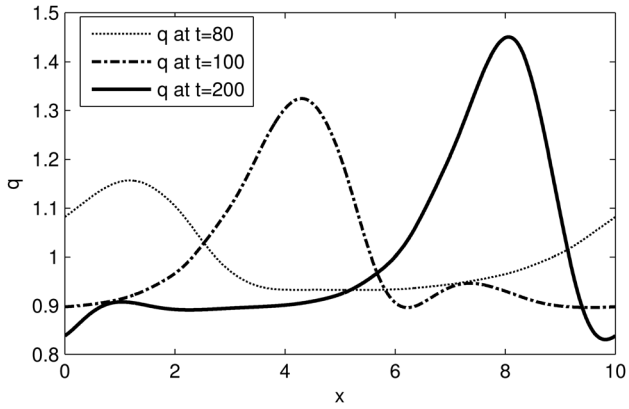

FIG. 16. Time evolution of q for a case with heating and permeability having $Re = 1.0$, $\delta = 0.1$, $\cot\ \beta = 0.5$, $We = 100$, $a_b = 0.2$, $Bi = Ma = 1$, and $\delta_1 = 0.1$. The WRM with the scaling $q_s = 1$ was used.

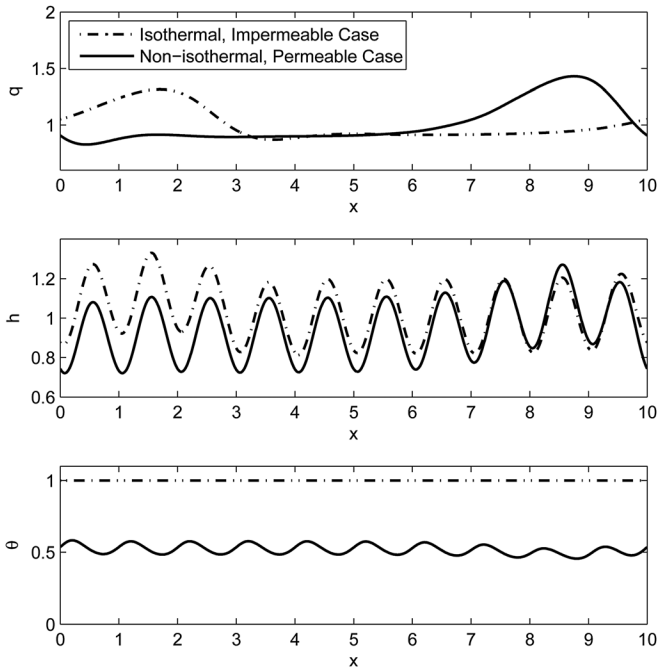

FIG. 17. Comparison between a case with heating and bottom permeability and an impermeable, isothermal case at t = 200. Both have $Re = 1.0$, $\delta = 0.1$, $\cot\ \beta = 0.5$, $We = 100$, $a_b = 0.2$, and a domain length of ten bottom wavelengths. The case with heating and permeability has $Bi = Ma = 1$ and $\delta_1 = 0.1$. The WRM with the scaling $q_s = 1$ was used.

In the second step, the diffusive and source terms are considered. The equations,

$$\begin{bmatrix} \dfrac{\partial q}{\partial t} \\ \dfrac{\partial \phi}{\partial t} \end{bmatrix} = \begin{bmatrix} \Psi_2 \\ \Psi_4 \end{bmatrix}, \tag{44}$$

are discretized using the Crank-Nicolson scheme and solved iteratively. An important point to note is that during the second step, h remains constant and is equal to the value computed from the first step. Overall, this method of solving the model equations is second order accurate in space and first order accurate in time.

This method computes the fluid thickness, volume flow rate, and interface temperature through ϕ at each time step, and in doing so tracks the evolution of the fluid interface and temperature with time. For a flow having a super-critical Reynolds number, numerical perturbations are added to destabilize the flow. These perturbations grow and form waves which interact and eventually produce a stable wave pattern. This wave pattern circles through the domain due to the periodic boundary conditions applied at the ends.

The development of the interface with time is shown in Fig. 16 for a case with bottom topography and permeability, surface tension, and heating. A perturbation having a wavelength equal to the length of the domain is superimposed on the steady-state solution for q, and used as an initial condition at $t = 0$. Since this is an unstable configuration, the perturbation amplifies initially and then ultimately forms a wave that maintains its shape as it continuously cycles through the domain.

The fully developed results for the same case are compared to results for the corresponding isothermal, impermeable case in Fig. 17. The resulting fully developed snapshot of the volume flow rate, fluid thickness, and interface temperature over the domain are shown in the figure at $t = 200$. The volume flow rate, shown in the top panel, indicates that the wave formed for the case with heating and permeability is slightly more pronounced than that for the isothermal, impermeable case. This is to be expected since it has already been shown that, in general, heating and permeability tend to destabilize the flow. The wave is also more pronounced due to the Marangoni effect, since surface tension is greatest where the fluid temperature is smallest which typically occurs at the crest of the wave. Fluid will be drawn to areas of higher surface tension, which will result in an increased thickness.

The middle panel shows the fluid thickness. Relating this to the q distribution in the panel above, we observe that the peaks in the q-wave correspond to a thicker fluid depth, which is a result of the increased volume flux. Comparing the basic case with the permeable bottom case, it can be seen that when the q values are approximately equal, the fluid thickness is greater for the isothermal, impermeable case. This is simply because the bottom slip condition results in a higher velocity for the permeable case, and since the volume flow rate is the same, the fluid layer is thinner for the permeable case.

The interface temperature, plotted in the bottom panel, shows a constant temperature for the isothermal case and a varying temperature for the case with heating. A dip in interface temperature occurs near the wave crest since the fluid layer is thicker, and therefore receives less heat from the bottom. This results in an interface temperature closer to the ambient temperature. The shift between the locations of the maximum fluid thickness and minimum interface temperature is also apparent in these results. As already pointed out in Fig. 4, the minimum temperature occurs further downstream than expected due to the bottom permeability.

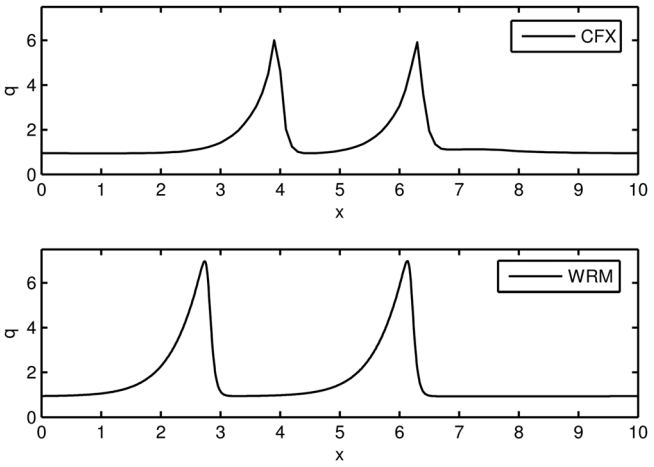

FIG. 18. CFX and WRM results for a case with porosity. The flow parameters are $Re = 1.75$, $\delta = 0.089$, $\delta_1 = 0.14$, cot $\beta = 1.38$, and $We = Ma = Bi = a_b = 0$.

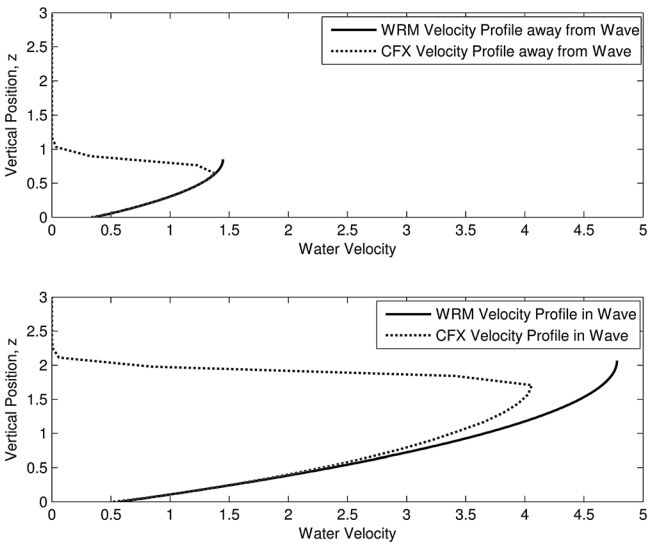

FIG. 19. CFX and WRM velocity profiles far from a wave (top) and at the peak of a wave (bottom). The flow parameters are $Re = 1.75$, $\delta = 0.089$, $\delta_1 = 0.14$, cot $\beta = 1.38$, and $We = Ma = Bi = a_b = 0$.

A. Comparison with CFX

The full Navier-Stokes equations for free surface flow down an inclined plane can be solved by employing the CFD software package CFX. The numerical method used by CFX to solve the governing equations is a combination of the finite volume and finite element methods. The domain is discretized into fluid elements, and control volumes are formed around element nodes. Momentum and mass are conserved over each control volume. Flow variables and fluid properties are stored at the nodes which are located within each control volume. The finite element method, using shape functions, is employed to calculate properties within fluid elements at the edges of the control volumes. The high resolution advection discretization scheme is used, which is a bounded second-order upwind scheme. It is bounded through the use of flux-limiting methods. A second-order backward Euler transient discretization scheme is used. To locate the free surface, a volume-of-fluid method is used. The volume fraction of one of the fluids is tracked as a solution variable using a volume fraction advection scheme. This causes a smearing of the interface due to numerical diffusion and the possibility of multiple adjacent cells containing a volume fraction between zero and one; however, CFX uses a compressive scheme to minimize this diffusion.

The numerical results from the weighted residual model are compared to those obtained using CFX for an isothermal case having a permeable even bottom. Heating was not included because CFX simulations with variable surface tension are problematic due to the mass loss that occurs. The flow parameters are $Re = 1.75$, $\delta = 0.089$, $\delta_1 = 0.14$, cot $\beta = 1.38$. The value of the permeability parameter is based on the values of Foametal A used in the experiments by Beavers and Joseph.[61] In CFX, the porous bottom is simulated by including a porous layer in the domain which is saturated with fluid. A momentum loss term is included in the governing equations to model the porous layer. This term is based on the permeability of the material and the volume fraction of solid material. Compared in Fig. 18 are the CFX and weighted residual model results. The figure shows that the number of peaks in the flow rate match. The spacing is similar, as are the height of the peaks, although the peaks in the weighted residual model results are slightly taller and farther apart. Other model simulations for the porous bottom problem match the corresponding CFX results fairly well. The results indicate that the weighted residual model continues to predict the flow well, even in cases with permeability.

The CFX results can also be used to compare the velocity profile predicted by the complete set of equations and boundary conditions with the profile assumed by the WRM. These velocity profiles are compared in Fig. 19. The CFX profile is calculated directly from the Navier-Stokes equations and is non-dimensionalized so as to compare it with the WRM profile given by Eq. (11), with the magnitude given by the WRM simulation results. Profiles at two locations are shown; those in the upper panel are far from a wave while those in the lower panel are at the peak of a wave. Far from a wave, the profiles match very well except near the interface. Near the interface, the CFX velocity decreases rapidly due to the smearing associated with the tracking of the free surface. As the volume fraction of liquid decreases over several cells, so does the liquid velocity. The profiles at the peak of the wave also agree well except near the interface. The noticeable difference in the maximum value is due to the difference in peak height shown in Fig. 18. These results indicate that the Beavers and Joseph slip condition is an effective way to model a permeable bottom and that the velocity profile assumed by the WRM mimics the actual velocity profile fairly well.

VIII. CONCLUSIONS

The method of weighted residuals was extended to solve the problem of gravity-driven flow over a porous, heated, wavy inclined surface. Although the focus of this study was

on surfaces that are sinusoidal, the equations were derived for arbitrary bottom topography. A constant bottom temperature was applied, and a variation of the Beavers and Joseph[61] slip condition was used to account for the non-planar permeable bottom. For the even bottom case, the critical Reynolds number calculated from a linear stability analysis of the model equations was compared to the result from the Benney equation, and the two were found to agree closely; good agreement was also found with the results of Sadiq *et al.*,[59] who used the Orr-Sommerfeld equation to predict the critical Reynolds number. This suggests that the WRM continues to make accurate predictions regarding the stability of the flow, even when the model is extended to include bottom heating and permeability. The expressions obtained for the critical Reynolds number indicate that heating and permeability acting alone destabilize the flow over an even bottom, as previously reported in the literature,[43,53,55] and that the interaction of these two effects is to further destabilize the flow. It was also found that increasing either bottom permeability or the Marangoni number monotonically destabilizes the flow for relevant values of the parameters. Although increasing the Biot number also destabilizes the flow, the behaviour is not monotonic. Instead, there is a specific Biot number, close to unity, for which the flow is most unstable. Lastly, allowing the density and viscosity to vary linearly with temperature does not alter the stability of the flow down an even impermeable heated incline for Weber numbers of order $1/\delta$, or larger, and Marangoni numbers of order unity, provided the variations in density and viscosity are comparable to those in surface tension.

The critical Reynolds number for flow over a wavy bottom, however, was found to depend on the Weber number. The observed trend was that, in general, bottom waviness stabilizes the flow for small Weber numbers, while for large Weber numbers bottom waviness was found to destabilize the flow. This is also consistent with previous findings for flows over impermeable surfaces.[10,14,43] Although a permeable bottom was found to destabilize the flow in most cases, the combination of strong surface tension, large bottom amplitude and bottom permeability can actually stabilize the flow.

As a final test of the WRM, numerical solutions of the full Navier-Stokes equations, computed using the CFX software package, were compared to the model predictions for isothermal flow with bottom permeability. The results obtained were found to agree closely, thus confirming that the WRM, when extended to include permeability, can predict the essential features of the flow. Additionally, the solutions of the full Navier-Stokes equations were used to compare its velocity profile to that assumed by the WRM. The two velocity profiles agreed reasonably well, further validating a key model assumption.

APPENDIX: TEMPERATURE DEPENDENT DENSITY AND VISCOSITY

The impact on the stability of the flow in allowing the density and viscosity to vary linearly with temperature according to

$$\frac{\rho}{\rho_0} = 1 - \hat{\Lambda}(T - T_a)$$

$$\frac{\mu}{\mu_0} = 1 - \hat{\lambda}(T - T_a)$$

is assessed below for the case of an even impermeable bottom. In this study, surface tension was allowed to vary according to

$$\frac{\sigma}{\sigma_0} = 1 - \frac{\gamma}{\sigma_0}(T - T_a).$$

It is interesting to note that in previous studies where surface tension was the only fluid property allowed to vary, little explanation was given to justify ignoring buoyancy and variable viscosity. Often a statement to the effect that for sufficiently thin films the influence of buoyancy can be neglected, is all that was included. The work by Goussis and Kelly[44] appears to be one of the earliest papers on inclined flow with variable surface tension which gives a more detailed explanation. They claim that for moderate values of the Prandtl number the effects of buoyancy will only be important for small inclination angles. The review paper by Oron *et al.*[22] mentions that for liquids with high viscosity the error made in ignoring the temperature variation may be significant, since viscosities can vary with an Arrhenius-type exponential temperature dependence. It appears that very little has been done on inclined flow with variable fluid properties. It is a complicated problem even for the impermeable and even bottom case. Goussis and Kelly[71] and Hwang and Weng[72] have included variable viscosity; however, these studies assume a prescribed constant temperature at the free surface, and thus, the Marangoni effect is not included. Kabova and Kuznetsov[73] include both variable viscosity and the Marangoni effect, but they only consider the steady-state problem.

Accounting for these variable fluid properties, and employing the Boussinesq approximation, the non-dimensional governing equations are as follows:

$$\frac{\partial u}{\partial x} + \frac{\partial w}{\partial z} = 0, \tag{A1}$$

$$\delta Re \frac{Du}{Dt} = -\delta Re \frac{\partial p}{\partial x} + 3(1 - \Lambda T) + \delta^2 \frac{\partial}{\partial x}\left[(1 - \lambda T)\frac{\partial u}{\partial x}\right] + \frac{\partial}{\partial z}\left[(1 - \lambda T)\frac{\partial u}{\partial z}\right] - \delta^2 \lambda \left(\frac{\partial T}{\partial x}\frac{\partial u}{\partial x} + \frac{\partial T}{\partial z}\frac{\partial w}{\partial x}\right), \tag{A2}$$

$$\delta^2 Re \frac{Dw}{Dt} = -Re \frac{\partial p}{\partial z} - 3\cot\beta(1 - \Lambda T) + \delta \frac{\partial}{\partial z}\left[(1 - \lambda T)\frac{\partial w}{\partial z}\right] - \delta^2 \lambda \left(\frac{\partial T}{\partial x}\frac{\partial u}{\partial z} + \frac{\partial T}{\partial z}\frac{\partial w}{\partial x}\right), \tag{A3}$$

$$\delta RePr \frac{DT}{Dt} = \delta^2 \frac{\partial^2 T}{\partial x^2} + \frac{\partial^2 T}{\partial z^2}, \tag{A4}$$

where $\frac{D}{Dt}$ denotes the two-dimensional material derivative, Re and Pr are defined as in Sec. II, but now in terms of ρ_0 and $\nu_0 = \mu_0/\rho_0$, and $\Lambda = \hat{\Lambda}\Delta T$ and $\lambda = \hat{\lambda}\Delta T$ represent dimensionless variation parameters for density and viscosity, respectively.

For flow over an even and impermeable incline the bottom conditions are

$$u = w = 0 \quad \text{and} \quad T = 1 \quad \text{at} \quad z = 0, \tag{A5}$$

while the conditions at the free surface are given by

$$\left.\begin{aligned} & p - \frac{2\delta}{Re}(1-\lambda T)\frac{\partial w}{\partial z} + \delta^2(We - MaT)\frac{\partial^2 h}{\partial x^2} = 0 \\ & (1-\lambda T)\frac{\partial u}{\partial z} - 4\delta^2\frac{\partial h}{\partial x}\frac{\partial u}{\partial x} + \delta^2\frac{\partial w}{\partial x} + MaRe\delta\left(\frac{\partial T}{\partial x} + \frac{\partial h}{\partial x}\frac{\partial T}{\partial z}\right) = 0 \\ & -BiT\left(1 + \frac{\delta^2}{2}\left[\frac{\partial h}{\partial x}\right]^2\right) = \frac{\partial T}{\partial z} - \delta^2\frac{\partial h}{\partial x}\frac{\partial T}{\partial x} \\ & w = \frac{\partial h}{\partial t} + u\frac{\partial h}{\partial x} \end{aligned}\right\} \quad \text{at} \quad z = h(x,t), \tag{A6}$$

where Bi, Ma, and We are defined as in Sec. II, but now in terms of ρ_0 and ν_0.

In this stability analysis, it will be assumed that the parameters Λ and λ are small, in particular they are taken to be $O(\delta)$. It is worth noting that this assumption is consistent with the parameter ranges considered in this study, and does not impose a severe restriction. To appreciate this, consider the ratio of the relative density variation to the relative surface tension variation given by

$$\frac{\text{density variation}}{\text{surface tension variation}} = \frac{\Lambda T}{\frac{\gamma \Delta T T}{\sigma_0}} = \frac{\Lambda We}{Ma}.$$

If $Ma = O(1)$ and We is of order $1/\delta$ or larger, then even if $\Lambda = O(\delta)$ the buoyancy variation would still be comparable to, or larger than, that in surface tension. A similar argument can also be made with regard to the assumption that the viscosity variation parameter, λ, is $O(\delta)$. Hence, it makes sense to set

$$\Lambda = \Lambda_1\delta, \quad \lambda = \lambda_1\delta.$$

To perform the linear stability analysis, the Benney equation is utilized. As explained in Sec. V A, this involves expanding u, w, p, and T in powers of δ as follows:

$$\begin{aligned} u &= u_0 + \delta u_1 + \cdots, \\ w &= w_0 + \delta w_1 + \cdots, \\ p &= p_0 + \delta p_1 + \cdots, \\ T &= T_0 + \delta T_1 + \cdots. \end{aligned}$$

Substituting these into Eqs. (A1)–(A4) and conditions (A5) and (A6) leads to a hierarchy of problems at various orders. The solutions emerging for the velocity components u and w can then be substituted into the kinematic condition to produce the Benney equation. To first order this equation is given by

$$\begin{aligned} & \frac{\partial h}{\partial t} + \frac{\partial}{\partial x}(h^3) + \delta\frac{\partial}{\partial x}\left[\frac{6Re}{5}h^6\frac{\partial h}{\partial x} + \frac{ReMaBi}{2}\frac{h^2}{(1+Bih)^2}\right. \\ & \left.\times\frac{\partial h}{\partial x} - \cot\beta h^3\frac{\partial h}{\partial x} + \frac{\delta^2 WeRe}{3}h^3\frac{\partial^3 h}{\partial x^3}\right] \\ & - \delta\left(\frac{\Lambda_1 h^2(9Bi^2h^2 + 28Bih + 24)}{8(1+Bih)^2}\frac{\partial h}{\partial x}\right. \\ & \left. - \frac{\lambda_1 h^2(9Bi^2h^2 + 20Bih + 12)}{4(1+Bih)^2}\frac{\partial h}{\partial x}\right) = 0. \end{aligned} \tag{A7}$$

Linearizing Eq. (A7) using $h = 1 + \hat{h}$ and introducing the perturbation $\hat{h} = h_0 e^{jkx}e^{\omega t}$ leads to a dispersion relation for the temporal growth rate ω which can be solved. The real and imaginary parts of ω are

$$\begin{aligned} \Re(\omega) = \frac{k^2\delta}{30(1+Bi)^2}\big(&-10k^2Re\delta^2WeBi^2 - 30\cot\beta Bi^2 \\ &+ 36ReBi^2 - 20k^2Re\delta^2WeBi - 60\cot\beta Bi \\ &+ 15MaReBi + 72ReBi - 30\cot\beta + 36Re \\ &-10k^2Re\delta^2We\big) \end{aligned}$$

and

$$\begin{aligned} \Im(\omega) = \frac{k}{8(1+Bi)^2}\big(&9\delta\Lambda_1Bi^2 - 24\delta\lambda_1 + 28\delta\Lambda_1Bi - 48Bi \\ &- 24 - 40\delta\lambda_1Bi + 24\delta\Lambda_1 - 24Bi^2 - 18\delta\lambda_1Bi^2\big), \end{aligned}$$

respectively.

It is evident that, while the expression for the imaginary part of ω contains Λ_1 and λ_1, the expression for the real part is independent of these parameters. Therefore, the neutral stability state, satisfying $\Re(\omega) = 0$, is not affected by the temperature dependent variations in density and viscosity. Thus, the critical Reynolds number for the onset of instability is independent of Λ_1 and λ_1 and is given by

$$Re_{crit}^{even} = \frac{\frac{5}{6}\cot\beta}{1 + \frac{5MaBi}{12(1+Bi)^2}},$$

which is in exact agreement with the theoretical value for flow down an even heated, impermeable, incline.[43]

[1]S. Alekseenko, V. Nakoryakov, and B. Pokusaev, "Wave formation on a vertical falling liquid film," AIChE J. **31**, 1446 (1985).
[2]N. J. Balmforth and S. Mandre, "Dynamics of roll waves," J. Fluid Mech. **514**, 1 (2004).
[3]T. B. Benjamin, "Wave formation in laminar flow down an inclined plane," J. Fluid Mech. **2**, 554 (1957).
[4]D. J. Benney, "Long waves on liquid films," J. Math. Phys. **45**, 150 (1966).
[5]R. R. Brock, "Development of roll-wave trains in open channels," J. Hydr. Div. **95**(HY4), 1401 (1969).
[6]B. S. Brook, T. J. Pedley, and S. A. Falle, "Numerical solutions for unsteady gravity-driven flows in collapsible tubes: Evolution and roll-wave instability of a steady state," J. Fluid Mech. **396**, 223 (1999).
[7]H.-C. Chang, "Wave evolution on a falling film," Annu. Rev. Fluid Mech. **26**, 103 (1994).
[8]H.-C. Chang, E. A. Demekhin, and E. Kalaidin, "Coherent structures, self-similarity and universal roll wave coarsening dynamics," Phys. Fluids **12**, 2268 (2000).
[9]R. V. Craster and O. K. Matar, "Dynamics and stability of thin liquid films," Rev. Mod. Phys. **81**, 1131 (2009).
[10]S. J. D. D'Alessio, J. P. Pascal, and H. A. Jasmine, "Instability in gravity-driven flow over uneven surfaces," Phys. Fluids **21**, 062105 (2009).
[11]L. A. Davalos-Orozco, "Nonlinear instability of a thin film flowing down a smoothly deformed surface," Phys. Fluids **19**, 074103 (2007).
[12]L. A. Davalos-Orozco, "Instabilities of thin films flowing down flat and smoothly deformed walls," Microgravity Sci. Technol. **20**, 225 (2008).
[13]T. Häcker and H. Uecker, "An integral boundary layer equation for film flow over inclined wavy bottoms," Phys. Fluids **21**, 092105 (2009).
[14]C. Heining and N. Aksel, "Bottom reconstruction in thin-film flow over topography: Steady solution and linear stability," Phys. Fluids **21**, 083605 (2009).
[15]C. Heining, V. Bontozoglou, N. Aksel, and A. Wierschem, "Nonlinear resonance in viscous films on inclined wavy planes," Int. J. Multiphase Flow **35**, 78 (2009).
[16]P. Julien and D. Hartley, "Formation of roll waves in laminar sheet flow," J. Hydraul. Res. **24**, 5 (1986).
[17]P. L. Kapitza and S. P. Kapitza, "Wave flow of thin layers of a viscous fluid. III. Experimental study of undulatory flow conditions," J. Exp. Theor. Phys. **19**, 105 (1949).
[18]C. Kranenburg, "On the evolution of roll waves," J. Fluid Mech. **245**, 249 (1992).
[19]J. Liu, J. D. Paul, and J. P. Gollub, "Measurements of the primary instabilities of film flows," J. Fluid Mech. **250**, 69 (1993).
[20]J. Liu, B. Schneider, and J. P. Gollub, "Three-dimensional instabilities of film flows," Phys. Fluids **7**, 55 (1995).
[21]A. A. Nepomnyaschy, "Stability of wave regimes in a film flowing down on inclined plane," Izv. Akad. Nauk SSSR, Mekh. Zhidk. Gaza **3**, 28 (1974).
[22]A. Oron, S. H. Davis, and S. G. Bankoff, "Long-scale evolution of thin liquid films," Rev. Mod. Phys. **69**, 931 (1997).
[23]A. Oron and C. Heining, "Weighted-residual integral boundary-layer model for the nonlinear dynamics of thin liquid films falling on an undulating vertical wall," Phys. Fluids **20**, 082102 (2008).
[24]T. Prokopiou, M. Cheng, and H.-C. Chang, "Long waves on inclined films at high Reynolds number," J. Fluid Mech. **222**, 665 (1991).
[25]B. Ramaswamy, S. Chippada, and S. W. Joo, "A full-scale numerical study of interfacial instabilities in thin-film flows," J. Fluid Mech. **325**, 163 (1996).
[26]C. Ruyer-Quil and P. Manneville, "Improved modeling of flows down inclined planes," Eur. Phys. J. B **15**, 357 (2000).
[27]C. Ruyer-Quil and P. Manneville, "Further accuracy and convergence results on the modeling of flows down inclined planes by weighted-residual approximations," Phys. Fluids **14**, 170 (2002).
[28]T. R. Salamon, R. C. Armstrong, and R. A. Brown, "Traveling waves on vertical films: Numerical analysis using the finite element method," Phys. Fluids **6**, 2202 (1994).
[29]B. Scheid, C. Ruyer-Quil, and P. Manneville, "Wave patterns in film flows: Modelling and three-dimensional waves," J. Fluid Mech. **562**, 183 (2006).
[30]V. Y. Shkadov, "Wave conditions in flow of thin layer of a viscous liquid under the action of gravity," Izv. Akad. Nauk SSSR, Mekh. Zhidk. Gaza **1**, 43 (1967).
[31]M. K. Smith, "The mechanism for the long-wave instability in thin liquid films," J. Fluid Mech. **217**, 469 (1990).
[32]H. Tougou, "Long waves on a film flow of a viscous fluid down an inclined uneven wall," J. Phys. Soc. Jpn. **44**, 1014 (1978).
[33]Y. Y. Trifonov, "Viscous liquid film flows over a periodic surface," Int. J. Multiphase Flow **24**, 1139 (1998).
[34]Y. Y. Trifonov, "Stability and nonlinear wavy regimes in downward film flows on a corrugated surface," J. Appl. Mech. Tech. Phys. **48**, 91 (2007).
[35]Y. Y. Trifonov, "Stability of a viscous liquid film flowing down a periodic surface," Int. J. Multiphase Flow **33**, 1186 (2007).
[36]R. Usha and B. Uma, "Long waves on a viscoelastic film flow down a wavy incline," Int. J. Non-Linear Mech. **39**, 1589 (2004).
[37]M. Vlachogiannis and V. Bontozoglou, "Experiments on laminar film flow along a periodic wall," J. Fluid Mech. **457**, 133 (2002).
[38]A. Wierschem and N. Aksel, "Instability of a liquid film flowing down an inclined wavy plane," Physica D **186**, 221 (2003).
[39]A. Wierschem, C. Lepski, and N. Aksel, "Effect of long undulated bottoms on thin gravity-driven films," Acta Mech. **179**, 41 (2005).
[40]A. Wierschem, T. Pollak, C. Heining, and N. Aksel, "Suppression of eddies in films over topography," Phys. Fluids **22**, 113603 (2010).
[41]C.-S. Yih, "Stability of liquid flow down an inclined plane," Phys. Fluids **6**, 321 (1963).
[42]B. Zanuttigh and A. Lamberti, "Roll waves simulation using shallow water equations and weighted average flux method," J. Hydraul. Res. **553**, 610 (2002).
[43]S. J. D. D'Alessio, J. P. Pascal, H. A. Jasmine, and K. A. Ogden, "Film flow over heated wavy inclined surfaces," J. Fluid Mech. **665**, 418 (2010).
[44]D. A. Goussis and R. E. Kelly, "Surface wave and thermocapillary instabilities in a liquid film flow," J. Fluid Mech. **223**, 25 (1991).
[45]S. W. Joo, S. H. Davis, and S. G. Bankoff, "Long-wave instabilities of heated falling films: Two dimensional theories of uniform layers," J. Fluid Mech. **230**, 117 (1991).
[46]S. Kalliadasis, E. A. Demekhin, C. Ruyer-Quil, and M. G. Velarde, "Thermocapillary instability and wave formation on a film falling down a uniformly heated plane," J. Fluid Mech. **492**, 303 (2003).
[47]S. Kalliadasis, A. Kiyashko, and E. A. Demekhin, "Marangoni instability of a thin liquid film heated from below by a local heat source," J. Fluid Mech. **475**, 377 (2003).
[48]S. P. Lin, "Stability of a liquid film down a heated inclined plane," Lett. Heat Mass Transfer **2**, 361 (1975).
[49]A. Mukhopadhyay and A. Mukhopadhyay, "Nonlinear stability of viscous film flowing down an inclined plane with linear temperature variation," J. Phys. D: Appl. Phys. **40** 5683 (2007).
[50]C. Ruyer-Quil, B. Scheid, S. Kalliadasis, M. G. Velarde, and R. Kh. Zeytounian, "Thermocapillary long waves in a liquid film flow. Part 1. Low-dimensional formulation," J. Fluid Mech. **538**, 199 (2005).
[51]A. Samanta, "Stability of liquid film falling down a vertical non-uniformly heated wall," Physica D **237**, 2587 (2008).
[52]B. Scheid, C. Ruyer-Quil, S. Kalliadasis, M. G. Velarde, and R. Kh. Zeytounian, "Thermocapillary long waves in a liquid film flow. Part 2. Linear stability and nonlinear waves," J. Fluid Mech. **538**, 223 (2005).
[53]P. M. J. Trevelyan, B. Scheid, C. Ruyer-Quil, and S. Kalliadasis, "Heated falling films," J. Fluid Mech. **592**, 295 (2007).
[54]R. Liu and Q. Liu, "Instabilities of a liquid film flowing down an inclined porous plane," Phys. Rev. E **80**, 036316 (2009).
[55]J. P. Pascal, "Linear stability of fluid flow down a porous inclined plane," J. Phys. D **32**, 417 (1999).

[56]J. P. Pascal, "Instability of power-law fluid flow down a porous incline," J. Non-Newtonian Fluid Mech. **133**, 109 (2006).
[57]J. P. Pascal and S. J. D. D'Alessio, "Instability in gravity driven flow over uneven permeable surfaces," Int. J. Multiphase Flow **36**, 449 (2010).
[58]U. Thiele, B. Goyeau, and M. G. Velarde, "Stability analysis of thin flow along a heated porous wall," Phys. Fluids **21**, 014103 (2009).
[59]I. Sadiq, R. Usha, and S. Joo, "Instabilities in a liquid film flow over an inclined heated porous substrate," Chem. Eng. Sci. **65**, 4443 (2010).
[60]I. Sadiq and R. Usha, "Thin Newtonian film flow down a porous inclined plane: Stability analysis," Phys. Fluids **20**, 022105 (2008).
[61]G. S. Beavers and D. D. Joseph, "Boundary conditions at a naturally permeable wall," J. Fluid Mech. **30**, 197 (1967).
[62]B. Scheid, C. Ruyer-Quil, U. Thiele, O. A. Kabov, J. C. Legros, and P. Conlinet, "Validity domain of the Benney equation including Marangoni effect for closed and open flows," J. Fluid Mech. **527**, 303 (2005).
[63]P. Rosenau, A. Oron, and J. Hyman, "Bounded and unbounded patterns of the Benney equation," Phys. Fluids A **4**, 1102 (1992).
[64]A. Oron and O. Gottlieb, "Subcritical and supercritical bifurcations of the first and second order Benney equations," J. Eng. Math. **50**, 121 (2004).
[65]J. M. Floryan, S. H. Davis, and R. E. Kelly, "Instabilities of a liquid film flowing down a slightly inclined plane," Phys. Fluids **30**, 983 (1987).
[66]P. Saffman, "On the boundary conditions at the surface of a porous medium," Stud. Appl. Math. **50**, 93 (1971).
[67]M. LeBars and M. Worster, "Interfacial conditions between a pure fluid and a porous medium: Implications for binary alloy solidification," J. Fluid Mech. **550**, 149 (2006).
[68]K. Nong and D. Anderson, "The film evolution over a thin porous layer: Modeling a tear film on a contact lens," SIAM J. of Appl. Math. **70**, 2771 (2010).
[69]R. J. LeVeque, *Finite Volume Methods for Hyperbolic Problems* (Cambridge University Press, Cambridge, 2002).
[70]R. J. LeVeque and H. C. Yee, "A study of numerical methods for hyperbolic conservation laws with stiff source terms," J. Comput. Phys. **86**, 187 (1990).
[71]D. A. Goussis and R. E. Kelly, "Effects of viscosity on the stability of film flow down heated or cooled inclined surfaces: Long-wavelength analysis," Phys. Fluids **28**, 3207 (1985).
[72]C.-C. Hwang and C.-I. Weng, "Non-linear stability analysis of film flow down a heated or cooled inclined plane with viscosity variation," Int. J. Heat Mass Transfer **31**, 1775 (1988).
[73]Y. O. Kabova and V. V. Kuznetsov, "Downward flow of a nonisothermal thin liquid film with variable viscosity," J. Appl. Mech. Tech. Phys. **43**, 895 (2002).